Chapter - 4

Impedance Matching and Bandwidth Enhancement in Hexagonal Planar Antennas

4.1. Introduction

Vertex fed hexagon planar antenna does not excite the lower mode as it can be concluded from analysis presented in chapter 2 and chapter 3. In this chapter, the parallel plate capacitor (PPC) is used to match the impedance, to excite the lowest mode of hexagonal patch. The bandwidth of the hexagonal planar antenna at lowest mode is also enhanced by using a thick dielectric substrate integrated with AMC.

Economic and efficient antennas with fundamental mode radiation are always in demand for modern wireless communication systems. Hexagonal patch antennas provide similar performance as rectangular and circular patches with an optimized feed point but with a lower patch area and a comparable gain (Joshi 2016a). Poor impedance matching is observed for lower order mode resonating near λ/4 when the feeding probe is in proximity to vertex of the hexagon. It is essential to identify a technique to excite lower order mode in hexagonal patch antenna for a uniform radiation pattern. Probe-fed hexagonal patch antennas have been earlier reported (Honggang 2016) (Wang 2016) and hexagonal geometries have been explored in frequency selective surfaces, fractal and annular geometries (Joozdani 2016) (Singhal 2016) (Saxena 2017). A perturbed hexagonal microstrip patch antenna was presented by Qian et al. (Qian 2011) for dual band application at 3.5 and 5.2 GHz. The polygonal patch antenna with reactive impedance ground plane for UMTS application (Bilotti 2006) was proposed by Bilotti et al.

Hexagonal patch antennas generally excite higher modes those resonates at 3λ/20 or lower wavelength instead of λ/4 and show broadband behaviour at high frequencies when fed at vertex (Joshi 2016b) (Joshi 2015b) (Sawant 2015) (Ghatak 2013). For a uniform and broader radiation pattern, it is necessary to excite lower modes. Probe reactance may be compensated through an annular gap or a PPC, as demonstrated earlier for thick substrates in reference (Manteghi 2009) (Kovitz 2014) respectively. This chapter utilizes one of the techniques highlighted in (Kovitz 2014) to compensate probe reactance when fed at vertex of hexagonal patch to excite fundamental mode at 2.4 GHz. PPC compensation is chosen over annular gap because instead of ring, an arc is formed around a vertex-fed probe. Due to this limitation of annular gap at the vertex, it will appear as if proximity feed is chosen over direct feeding.

Frequency selective surfaces (FSS) are used as high pass, low pass, band pass and band stop surfaces for electromagnetic shielding (Celozzi 2008). FSS are also known as high impedance surfaces and artificial magnetic conductor (Munk 2000). AMC with different popular shapes such as loop, jerusalem crosses, meander line based and spiral shaped has been explored by many researchers (Mittra 1988) . The loop AMC with square geometry are analyzed and presented for band stop applications and spurious rejection (Mittra 1988) (Lu 2009) (Liu 2017) (Barrera 2017) (Nasrollahi 2017) (Liu 2018). The square loop AMC is analysed using numerical method (Gombor 2015), electromagnetic scattering (Mittra 1988), equivalent circuit model (Varkani 2018) out of which the circuit modelling is fast and easy to analyze square loop AMC. The band reject frequency response of the square AMC depends on the dimensions and dielectric use to support AMC. Barrera et al. proposed numerical model to estimate the effective permittivity for square loop AMC (Barrera 2017). Ferreira et al. proposed an improvised formula to calculate effective dielectric constant of loop and slot AMC for TE wave incidence (Ferreira 2015). It is very necessary to carefully calculate the effective dielectric constant for TE and TM wave incidence separately. The physical parameter of the square loop AMC with different inner widths are chosen in order to check its band stop frequency response at two separate frequency at TE and TM incidence wave. The effective dielectric constant is calculated for TE and TM wave incidence with expressions suggested in literatures. This research is useful where separation between two near bands is required. AMC are utilized for separation of two closely spaced GSM bands (Kartal 2017). The analysis techniques of loop AMC with different inner width are not much explored for TE and TM incident wave. The effect of dielectric constant on band stop resonant frequency is deeply analyzed and appropriate expression for effective dielectric constant calculation for TE and TM incident wave is suggested in this chapter. This research will be useful for researchers to estimate the transmittance of AMC for both TE and TM wave incidence in a more effective and easier way.

A vertex-fed slotted hexagonal antenna with PPC is demonstrated and analysed to study the effect of PPC on probe reactance and antenna far-field radiation characteristics. A thin dielectric substrate with thickness less than λ/10 is used to develop the antenna and analysis is done over the obtained results through measurements. The chapter demonstrates a method to improve impedance matching for lower mode, suppressed due to geometry of hexagon and feed location, by introducing PPC with probe feed. The objective here, in this chapter, is to identify a technique which results in $|S_{11}| < -10$ dB at imperfect feed locations e.g. when probe is fed near to vertex of the hexagon. Capacitive probe compensation using a circular disk of FR-4 sandwiched between two copper discs is found to be a suitable choice.

A square loop AMC with different inner widths is demonstrated. The effect of AMC on transmittance is analyzed and studied in the second section of the chapter. The transmittance effect of AMC on various parameters such as loop dimension, inner width dimension using circuit modelling when TE and TM wave is incident are studied and analysed. The measurement setup for transmittance measurement is discussed in third section of the chapter.

The AMC is developed on thin FR-4 dielectric substrate and transmission measurements are presented in the fourth section. The main purpose of this work is to demonstrate a method to achieve high rejection. The last section deals with the significant contributions of demonstrated work.

In this chapter lower mode excitation in probe fed hexagonal antenna and bandwidth is enhanced using combination of thick substrate and AMC. Section 4.2 demonstrate the lower mode of probe fed hexagonal patch is excited using PPC technique. The AMC modelling for TE and TM wave incidence is discussed in section 4.3. Finally, in section 4.4 the bandwidth of the probe fed hexagonal patch antenna is enhanced using thick dielectric substrate and AMC. A method to improve the radiation bandwidth in directly fed hexagonal patch by introducing AMC array and PPC for applications like Wi-Fi is demonstrated in section 4.4.

4.2. Lower Mode Excitation in Vertex-Fed Slotted Hexagonal Antenna

The slotted hexagonal antenna with circular PPC and a 37 × 37 mm^2 sized ground plane is designed as shown in Figure 4.1. Glass epoxy FR-4 substrate (ε_r = 4.3, tan δ = 0.025) is the substrate material used for design and development of the antenna with a thickness of 1.5 mm and an overall dimension of 50 × 50 mm^2. The hexagonal patch antenna is designed using half wavelength, $\lambda_g/2$ where, the guided wavelength, λ_g = 60 mm at 2.5 GHz. To resonate at 2.4 GHz, dimensions of the hexagonal patch are further optimized to 35 mm × 30.3 mm which are comparable to $\lambda_g/2$. The hexagonal patch size is 35 × 30.3 mm^2 with a circumradius of 17.5 mm in all experiments with a hexagonal slot size of 6 × 5.2 mm^2.

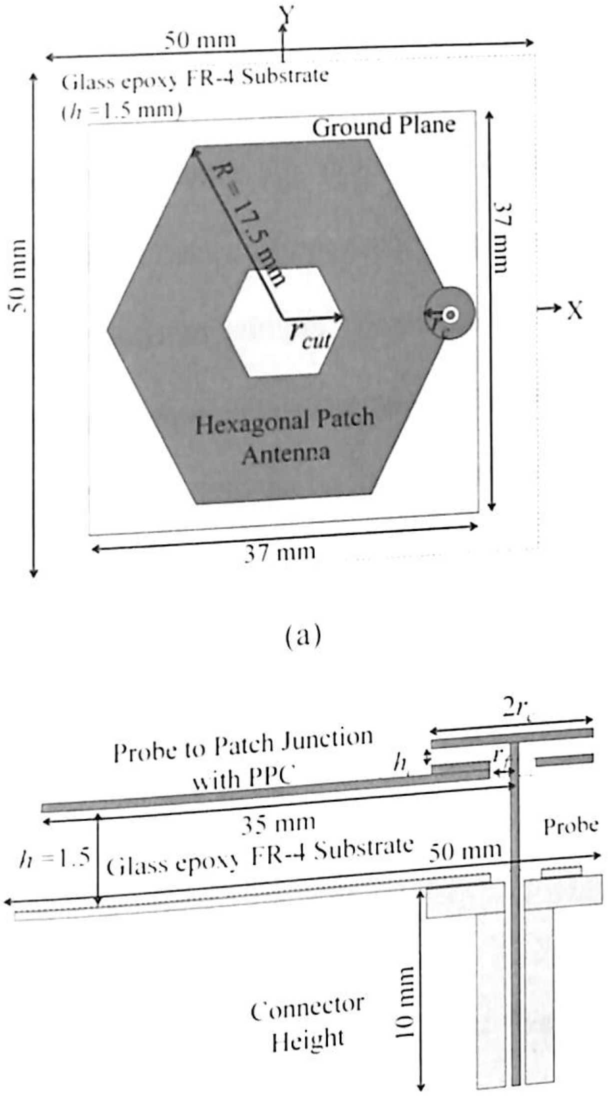

(a)

(b)

Figure 4.1. Structure of Proposed slotted hexagonal antenna with PPC (a) Layout with dimension (b) Side view.

The vertex of the hexagon is fed through a SMA connector after applying simulation and analysis as suggested in (Joshi 2015d) (Joshi 2016b). The pin radius of the SMA connector is 0.62 mm; the radius of dielectric in connector is 2.076 mm while the 10 mm long outer conductor has a radius of 2.565 mm. The optimum value of circumradius of the hexagonal slot i.e. r_{cut} = 3 mm is obtained using technique applied in (Joshi 2016b). The circular PPC is developed by using a small disc of 4 mm radius of a double sided copper clad with a single layer substrate in-between and placing it around the probe feed above the vertex of hexagonal patch. For the antenna to radiate efficiently the impedance should be matched to the characteristics impedance of transmission line. Different experiments are performed to establish the technique to match impedance for the lowest order mode. Three different prototypes are developed to compare effect on impedance in presence and absence of PPC. Antenna A_1 is a hexagonal patch antenna without compensation capacitor while probe is directly fed at vertex. Antenna A_2 is same antenna arrangement as A_1 but now with a PPC with radius 4 mm and of height 1.5 mm. Antenna A_3 is again the same antenna arrangement used as A_2 but height of the PPC is now reduced to 0.94 mm.

The effective value of hexagonal circumradius, R_{eff} can be used to determine the resonant frequencies of the hexagonal patch antenna at different radiation modes using equation (4.1) of a circular patch antenna as given in (Ray 2007).

$$f_r = \frac{c k_{mn}}{2\pi R_{eff}\sqrt{\varepsilon_{eff}}} \tag{4.1}$$

where, m = 0, 1, 2, 3; n = 1 for first four modes. The first four values of k_{mn} are k_{11} = 1.841, k_{21}= 3.054, k_{01} = 3.832, k_{31}=4.201, c is speed of light, R_{eff} = 18.1 mm is effective radius and ε_{eff} = 3.957 is effective dielectric constant as defined in (Ray 2007).

The frequencies at which the first four modes are radiating, when calculated for designed hexagonal patch antenna using equation (4.1) are found to be 2.422 GHz, 4.018 GHz, 5.0416 GHz and 5.52 GHz for circular patch equivalent modes TM_{11}, TM_{21}, TM_{01} and TM_{31} respectively. The above values obtained using equation (4.1) are confirmed through measurement results presented in Figure 4.2 and Figure 4.6.

With an objective to establish $|S_{11}| < -10$ dB at 2.4 GHz, a PPC is placed over the probe of antenna, A_1 to form antenna, A_2. A thicker PPC of r_c = 4 mm with h_c = 1.5 mm is used with antenna, A_2 and $|S_{11}| \cong -10$ dB is observed. Further, when a slightly thinner PPC with h_c = 0.94 mm is used for antenna A_3, the objective of S_{11} less than -10 dB at 2.4 GHz is accomplished as reflected in Figure 4.2. It is observed that PPC with reduced thickness can improve reflection coefficient at a lower mode. The impedance at vertex is very high in the order of hundred of ohms as may be observed in Figure 4.3(a) in case of A_1. In order to match the input impedance of hexagon to the characteristics impedance of the coaxial line, a capacitor in series is required to compensate the real and reactive part of the hexagonal patch. Probe feeding increases value of impedance but inclusion of PPC compensate the increase in impedance due to feed location.

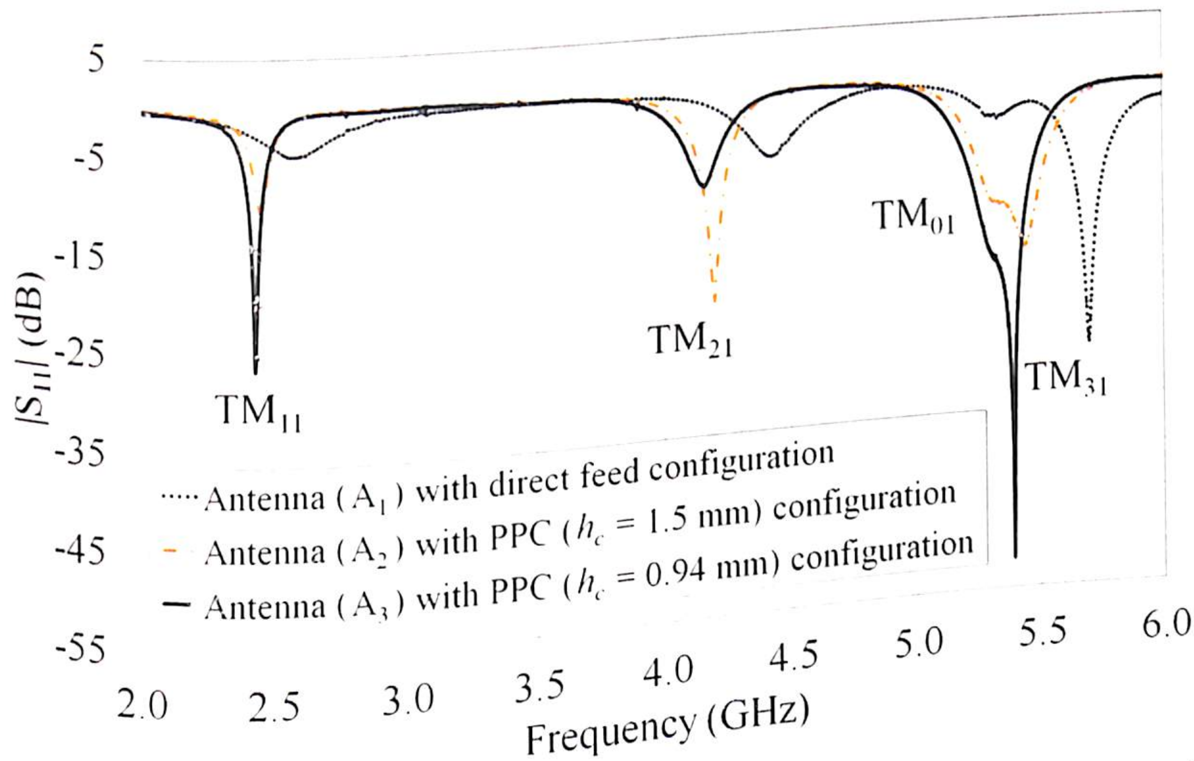

Figure 4.2. Measured Reflection coefficient (in dB) (S11) of different antenna (A1 - A3) configurations.

The impedance, Z_{11}, both real part and imaginary part are obtained from measurements of different antenna configurations (A_1-A_3). The real and imaginary impedances are compared as shown in Figure 4.3 (a) and (b) respectively.

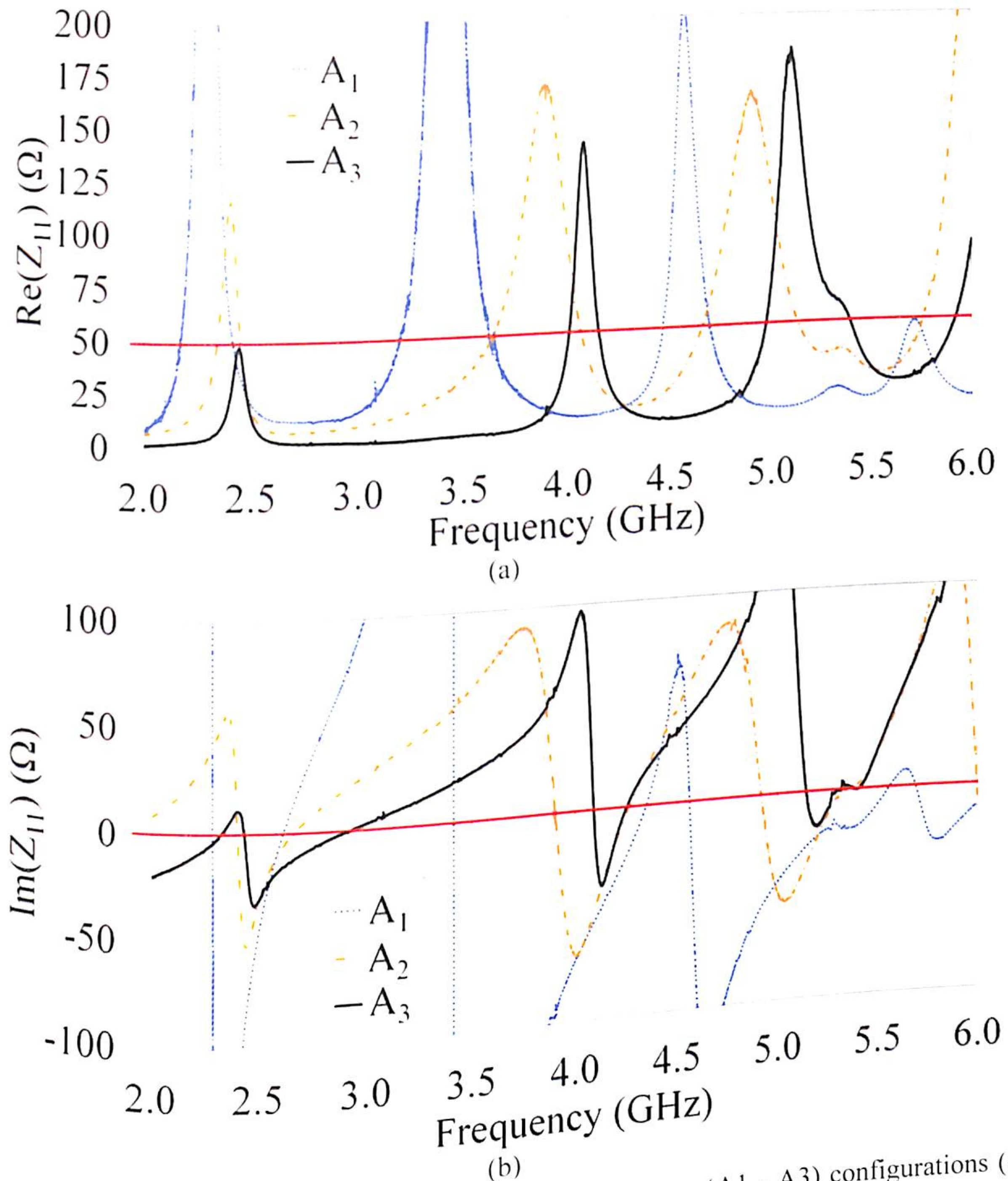

Figure 4.3. Measured Impedance (Z_{11}) of different antenna (A1 - A3) configurations (a) Real Impedance ($Re(Z_{11})$) (b) Imaginary Impedance ($Im(Z_{11})$).

Impedance, Z_{11} for antenna, A_3 at 2.4 GHz is approximately 45.4 - 0.7j Ω when PPC of radius, r_c = 4 mm and height, h_c = 0.94 mm is used. The phenomenon of impedance matching in presence and absence of PPC in hexagonal antenna can be observed in Figure 4.3. The effect of PPC in matching impedance due to imperfect feed location i.e. at vertex can be observed in case antenna A_3 with PPC having a real part of 45.4 Ω which is close to 50 Ω.

Also, presence of PPC decreases imaginary part of impedance Z_{11} to almost zero as shown in Figure 4.3(b). It is well known that at resonance, $X_L = X_C$. The upper plate of PPC to which probe feed is soldered provides a uniform circular surface compared to vertex of hexagon, thus decreasing real part of impedance Z_{11} to almost 50 Ω.

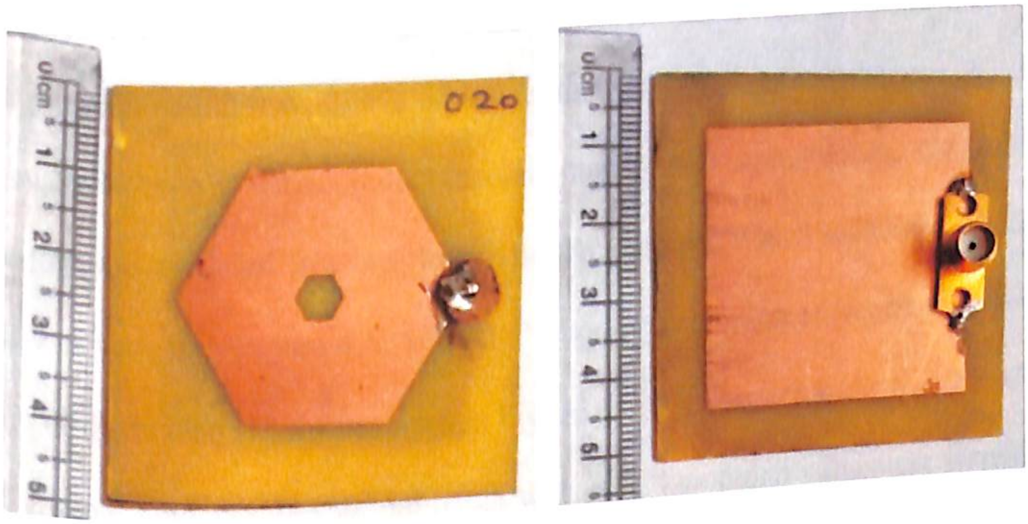

Figure 4.4. Picture of the developed antenna, A3 (a) Front (b) Back.

The developed slotted hexagonal antenna with PPC, using standard PCB development techniques, is shown in Figure 4.4. The developed antenna is very compact with an overall dimension of 50×50 mm^2.

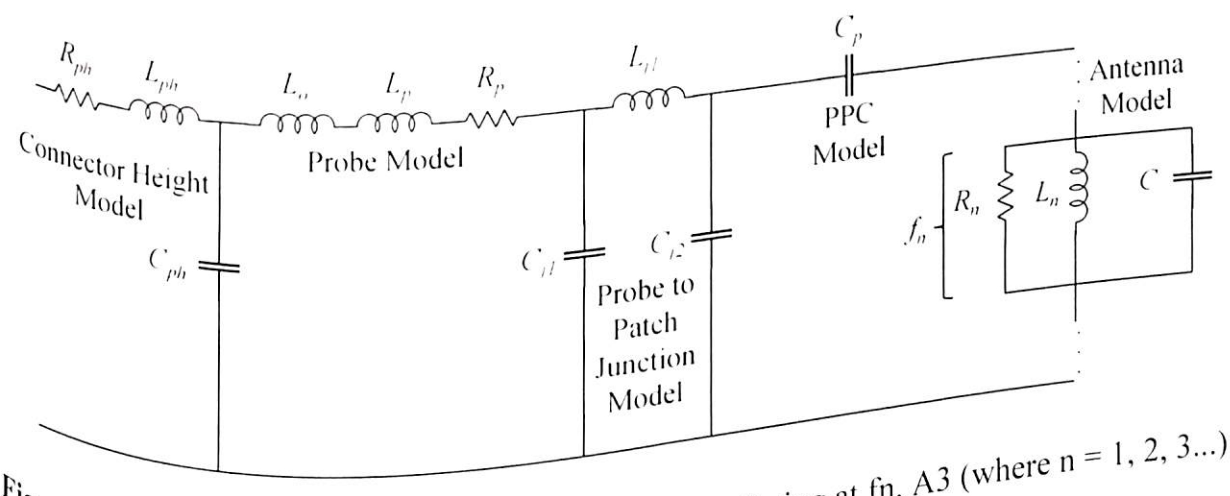

Figure 4.5. Equivalent circuit model of antenna radiating at fn, A3 (where n = 1, 2, 3...)

To explain the mechanism of the proposed antenna with probe compensation, an equivalent circuit is modeled using typical mathematical and analytical methods along with a simulation platform e.g. MATLAB and presented in Figure 4.5. The complex probe model consists of the probe height model, the probe model and the probe to patch junction model. The inductance due to probe height, L_{ph} is due to the inner conductor of the probe height with resistance, R_{ph} while C_{ph} is the capacitance developed between the inner and outer conductor separated by Teflon dielectric of the probe height. The probe model is due to the inner conductor of the probe which is inserted in the substrate with height h via hole to connect the patch. The pin with length h will have an inductance, $L_o + L_p$ and a resistance, R_p. The probe to patch junction have a series inductance, L_j and shunt capacitances, C_{j1} and C_{j2}. The proposed antenna is modeled as a simple parallel RLC circuit which resonates at a frequency, f_1 = 2.4 GHz as shown in Figure 4.5. The RLC circuits resonating at frequency, f_2 = 4.2 GHz and f_3 = 5.4 GHz are also shown in series in Figure 4.5. The capacitance, C = 9.8 pF is due to overlap of ground plane and hexagonal patch with slot. The tuned values are shown in Table 4.1.

Table 4.1. Values of lumped elements of equivalent circuit model of A3

Model	*Connector Height Model*			*Probe Model*			*Probe to Patch Junction Model*		
Parameters	R_{ph}	L_{ph}	C_{ph}	L_o	L_p	R_p	C_{j1}	L_j	C_{j2}
Values	0.04 Ω	2.42 nH	0.97 pF	0.11 pH	1.37 nH	7.16 Ω	2.4 pF	3.5 nH	2.8 pF
Model	*PPC Model*	*Antenna Model*							
Parameters	C_p	C	L_1	R_1	L_2	R_2	L_3	R_3	
Values	1.97 pF	9.8 pF	0.41 nH	261.26 Ω	0.13 nH	597.4 Ω	80 pH	118 Ω	

The expressions used for calculations of values of lumped circuit elements are available in (Joshi 2016b) (Garg 2001). The calculated values of the lumped circuit elements are indicated in Table 4.1.

Lower order modes are suppressed due to impedance mismatch between excitation and hexagonal patch antenna when directly fed through a probe. The high value of probe inductance and location of feed dominates impedance, Z_{11}. A capacitor between the probe and the vertex of the hexagonal patch antenna compensates the inductive effect and improves impedance matching at feed. The PPC connected in series excites fundamental mode in vertex-fed hexagonal patch antenna. Since height of PPC, $h_c < h$, height of antenna substrate, capacitance, C_p can be estimated using equation (4.2). Equation (4.2) is an alternate version of a equation used in (Kovitz 2014) where capacitance, C_p is calculated for two metal circular disk with radius, r_c while lower disk has a hole with radius, r_f separated by FR-4 dielectric material.

$$C_p = \frac{\varepsilon_0 \varepsilon_r (r_c^2 - r_f^2)}{h_c} \tag{4.2}$$

The compensation capacitance, C_p is found to be 1.97 pF using equation (4.2) for a substrate height, h_c = 0.94 mm, compensation capacitor radius, r_c = 4 mm and a circular slot radius, r_f = 0.75 mm as shown earlier in Figure 4.1(b).

Reflection coefficient ($|S_{11}|$ (dB)) obtained from equivalent circuit model is compared with VNA measured results in Figure 4.6. The measurement $|S_{11}|$ (dB) results display a -10 dB impedance bandwidth of 2.3 % from 2.387 to 2.442 GHz while equivalent circuit model reflects a similar band for C_p = 1.97 pF. There is a quantative difference in circuit analysis and measurement results for antenna, A_3 due to choice of resonant frequency during circuit modeling.

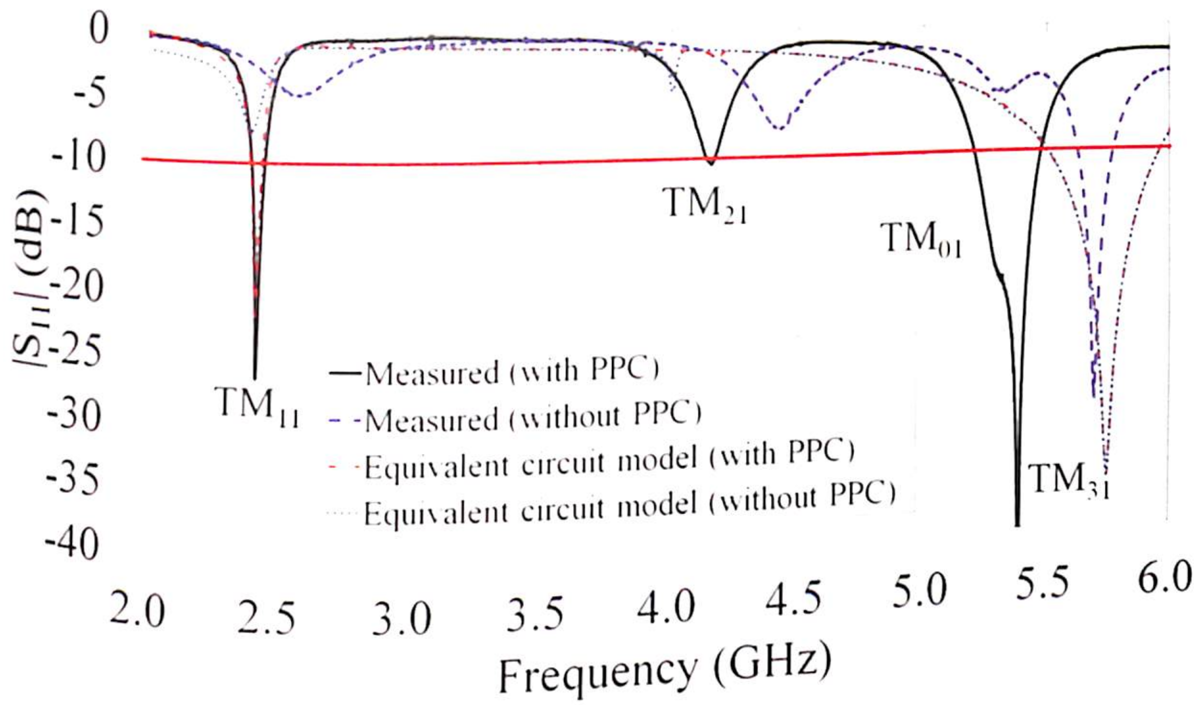

Figure 4.6. Measured Reflection coefficient (in dB) (S_{11}) of antenna with and without PPC compared with equivalent circuit model.

Other than the *RLC* resonators, all other circuit elements are modeled at 4 GHz, i.e. the centre frequency of the observation band from 2 GHz to 6 GHz. The value of C_p in equivalent circuit model can be further increased to 2.22 pF to obtain $|S_{11}| \cong$ -35 dB by decreasing h_c. This phenomenon can be observed in Figure 4.8. Real and imaginary impedance (Z_{11}) obtained from equivalent circuit model is also compared with VNA measured results in Figure 4.7(a) and (b) in order to show the phenomenon of impedance matching. The compensation capacitance, C_p is optimized using equivalent circuit modeling by varying the height of the capacitor, h_c, as h_c depends on C_p as given in equation (4.2). The height of the PPC, h_c is optimized by varying it from 1.5 to 0.5 mm as shown in Figure 4.8. Although $|S_{11}|$ $\cong$ -35 dB is achieved with introduction of PPC at vertex-feed, change in impedance bandwidth is not observed.

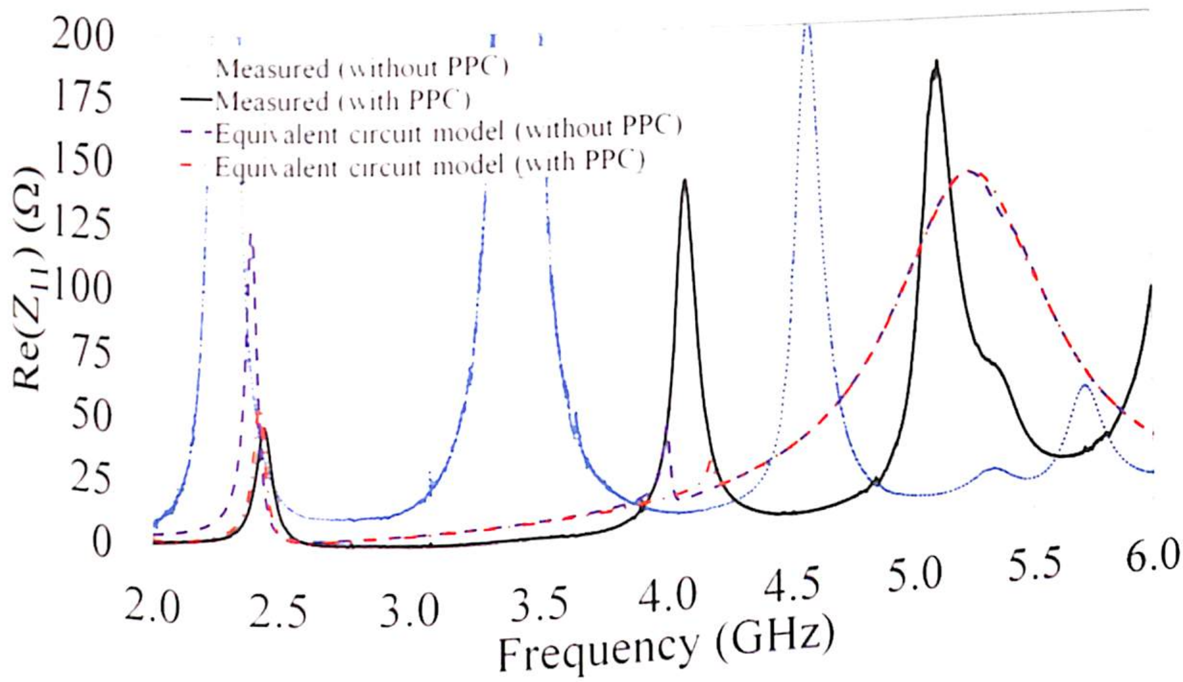

(a) Real Impedance (Re(Z_{11}))

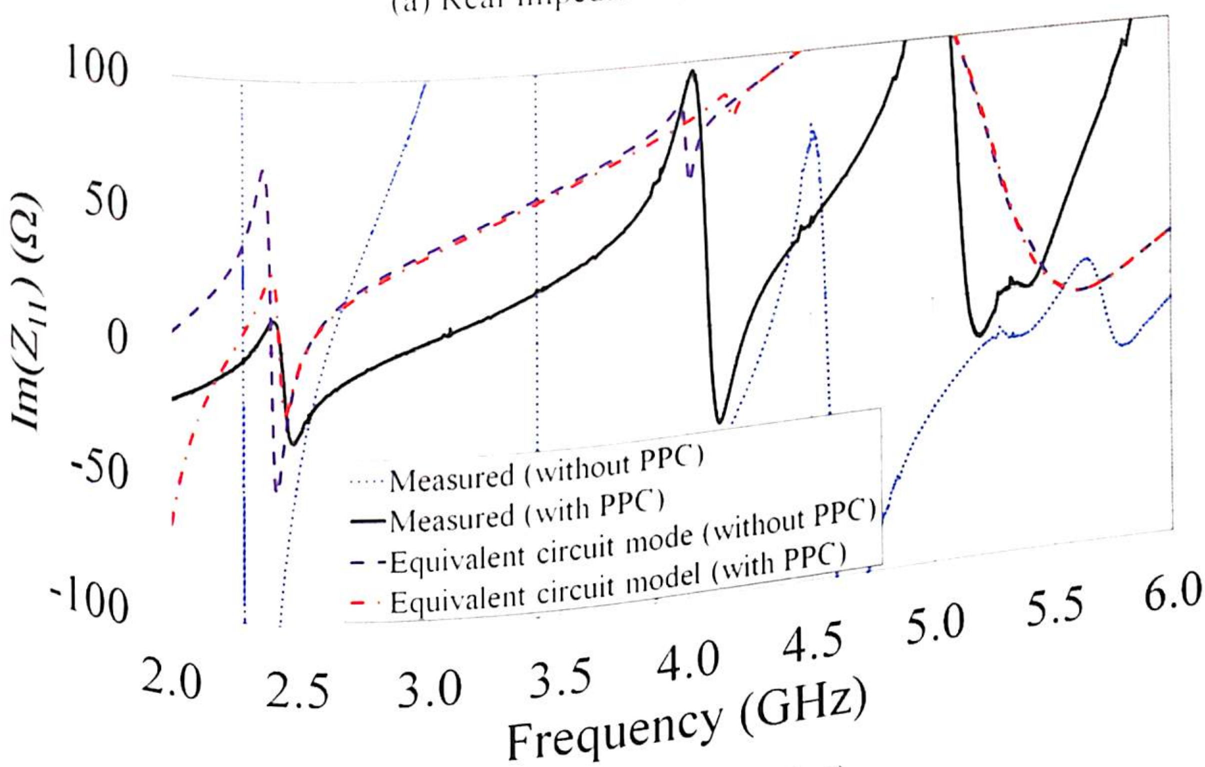

(b) Imaginary Impedance (Im(Z_{11})).

Figure 4.7. Measured Impedance (Z_{11}) of antenna with and without PPC compared with equivalent circuit model.

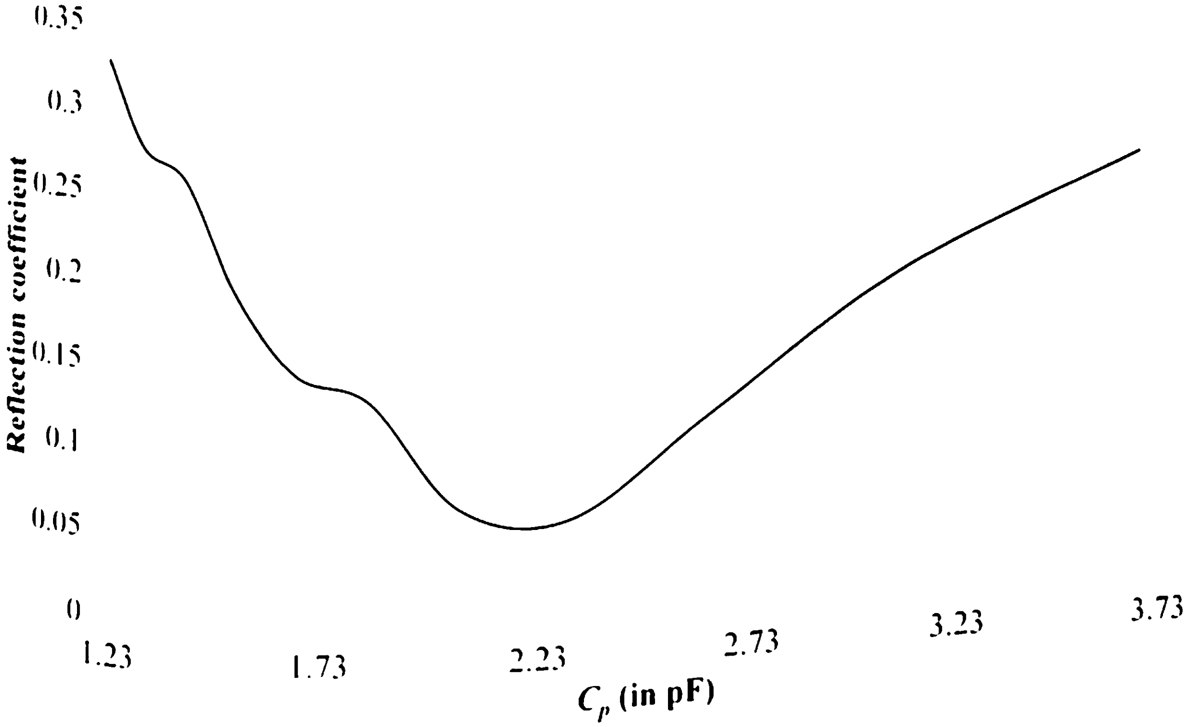

Figure 4.8. Calculated Reflection coefficient (magnitude) (S_{11}) of the compensation capacitor (Cp), where h_c varies from 1.5 to 0.5 mm.

The modal characteristics of the proposed antenna are also verified using the magnetic mode field ($\vec{H}$-field) with two different phases of excitation signal i.e. 90° and 270° at resonating frequency of 2.4 GHz and displayed in Figure 4.9(a) and 4.9(b). The magnetic mode field analysis suggests that the maximum $\vec{H}$-field is at the overlapping area of the hexagon with the ground. The magnetic mode field analysis suggest that the antenna radiates TM_{11} mode because the $\vec{H}_{mn}$vector is present on the XY plane and $\overrightarrow{H_z} = 0$, only one half wave variation is along the X-axis and no variation is along the Y-axis as observed from Figure 4.9(a) and 4.9(b).

The magnetic mode field of the hexagon as shown in Figure 4.9(a) which is unidirectional at phase 90° of the excitation signal, and the vector is pointing toward the negative Y-axis. The magnetic mode field is pointing toward the positive Y-axis in the phase reversal 270° as observed from Figure 4.9(b).

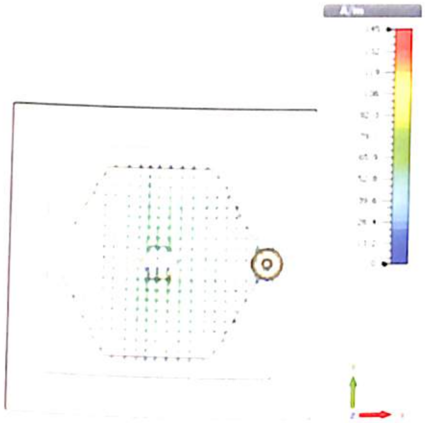

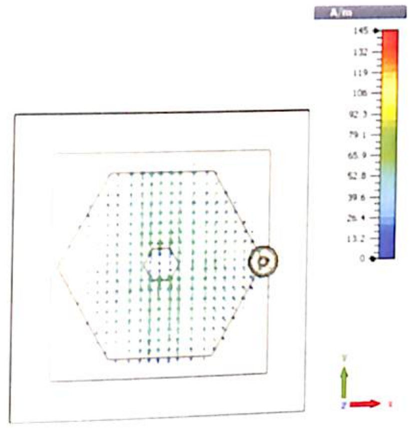

(a) 90° at 2.4 GHz (b) 270° at 2.4 GHz

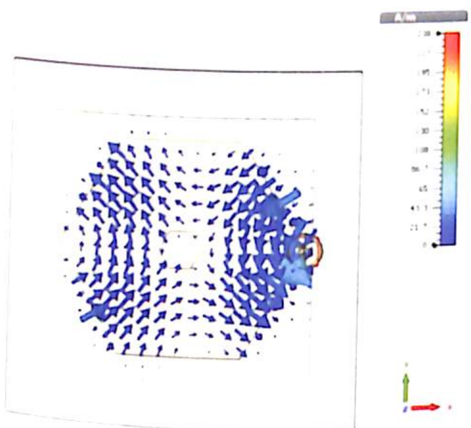

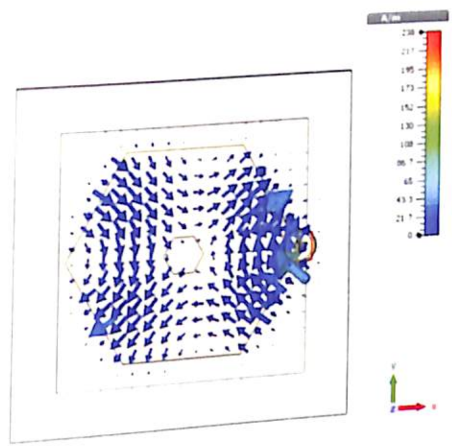

(c) 90° at 4.2 GHz (d) 270° at 4.2 GHz

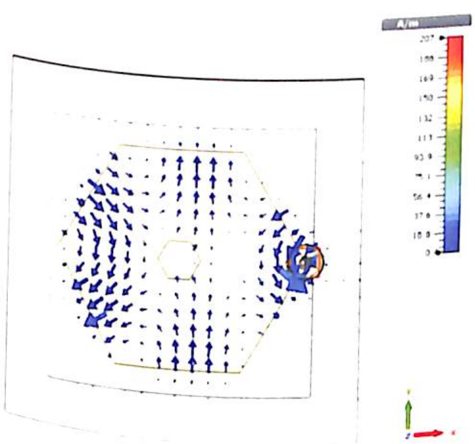

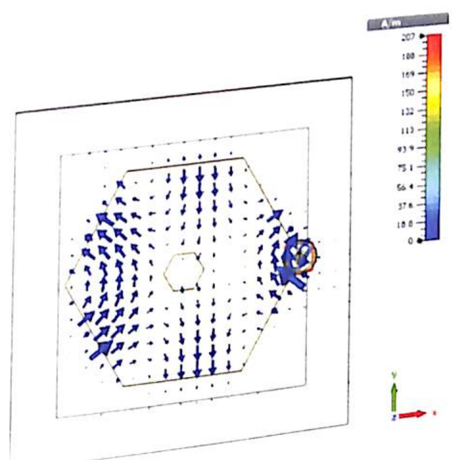

(e) 90° at 5.4 GHz (f) 270° at 5.4 GHz

Figure 4.9. Magnetic mode field of the antenna (A3) at three frequencies 2.4 GHz, 4.2 GHz and 5.4 GHz at two different phase of excitation signal 90° and 270°.

At 90° and 270° phase the magnetic mode field are created within the hexagon overlapping with the ground as shown in Figure 4.9(a) and 4.9(b). Similarly magnetic mode field is shown at 4.2 and 5.4 GHz in Figure 4.9(c), 4.9(d), 4.9(e) and 4.9(f). The magnetic mode field analysis at 4.2 GHz suggests that the antenna possess TM_{21}.

The broadband behaviour at 5.3 and 5.4 GHz is due to combination of two different modes i.e. TM_{01} and TM_{31} respectively, shown together in Figure 4.9(e) and 4.9(f). Due to mode overlap at 5.4 GHz, it is observed that although the impedance bandwidth is enhanced but eventually decreases the radiation efficiency and consequently decreases the farfield gain at higher mode.

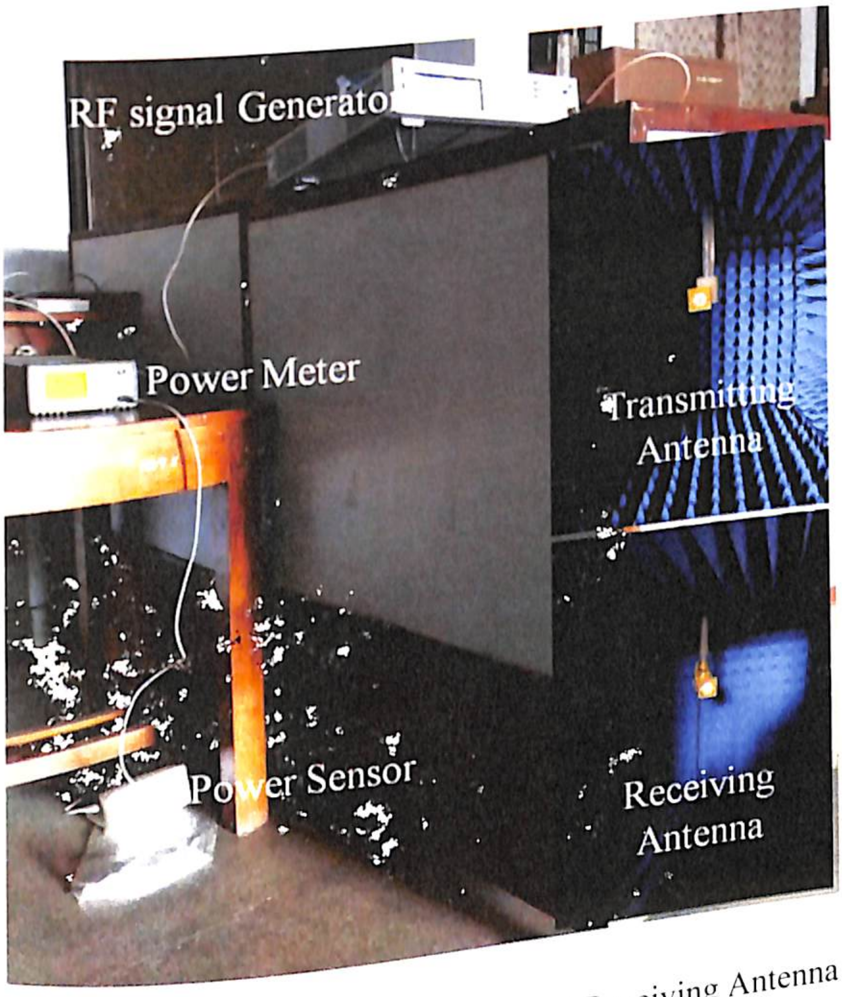

Figure 4.10. Measurement Setup [Transmitting and Receiving Antenna in Inset].

The radiation pattern is measured in an anechoic environment at 2.4 GHz using two identical (A_3) antennas and the measurement setup is shown in Figure 4.10 was earlier used and presented in chapter 3, Figure 3.31. The measurement setup involves received power being sensed by a CW Power Sensor (Agilent E-4412A) and measured by a Power Meter

(Agilent E-4418B) while the transmitting antenna is excited through a RF Signal Generator (Keysight N5173B).

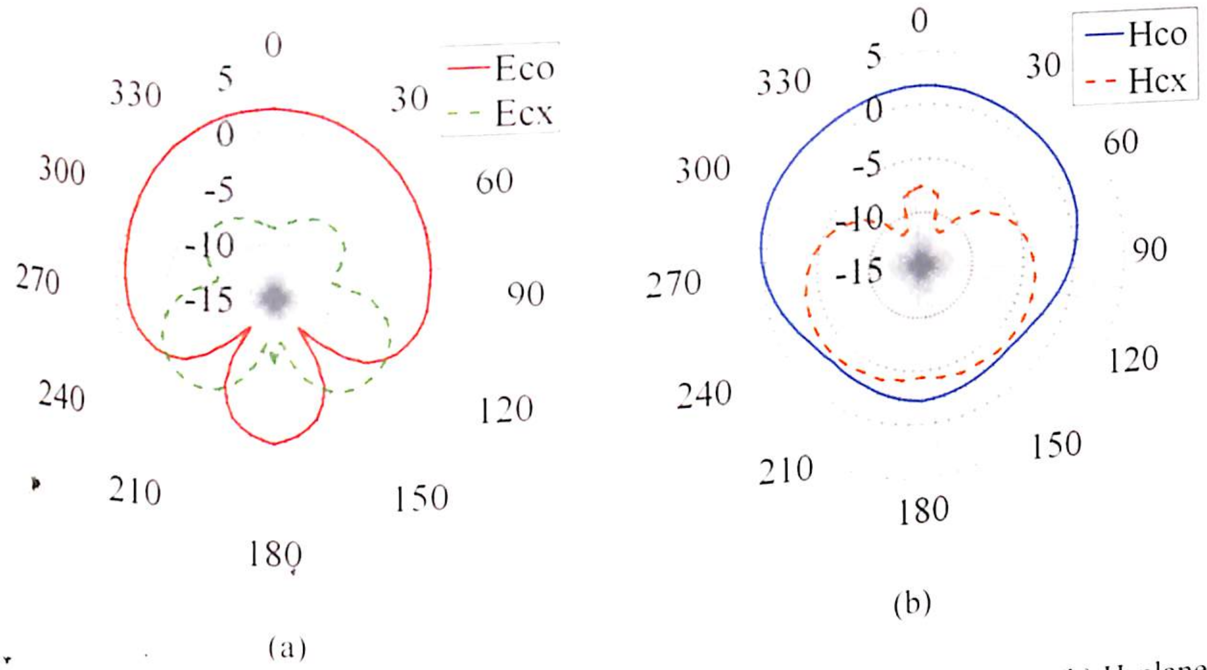

Figure 4.11. Antenna gain (dB) (Co- and Cross-polar) at 2.4 GHz (a) E-plane (b) H-plane.

The antenna at receiving end is rotated from 0° to 360° in 5° increments for received power measurements. The difference between power from the RF signal generator and the received power is around 15 dB when the distance between both the antennas used in setup for measurement is 90 cm including losses due to cable and connectors. The measured co-polarized (Eco/Hco) and cross-polarized (Ecx/Hcx) radiation patterns at 2.4 GHz for the E-plane and H-plane are shown in Figure 4.11. The gain of antenna, A_3 is calculated using Friss transmission equation and is equal to 2.11 dB in the main lobe direction. Around 10 dB difference between the co- and cross-polar levels in the main lobe direction is observed at 2.4 GHz in both E- and H-plane.

4.3. Modeling of Square Loop AMC with Different Edge Widths

The square loop AMC design with different inner widths and without vias is selected for analysis as shown in Figure 4.12(a).

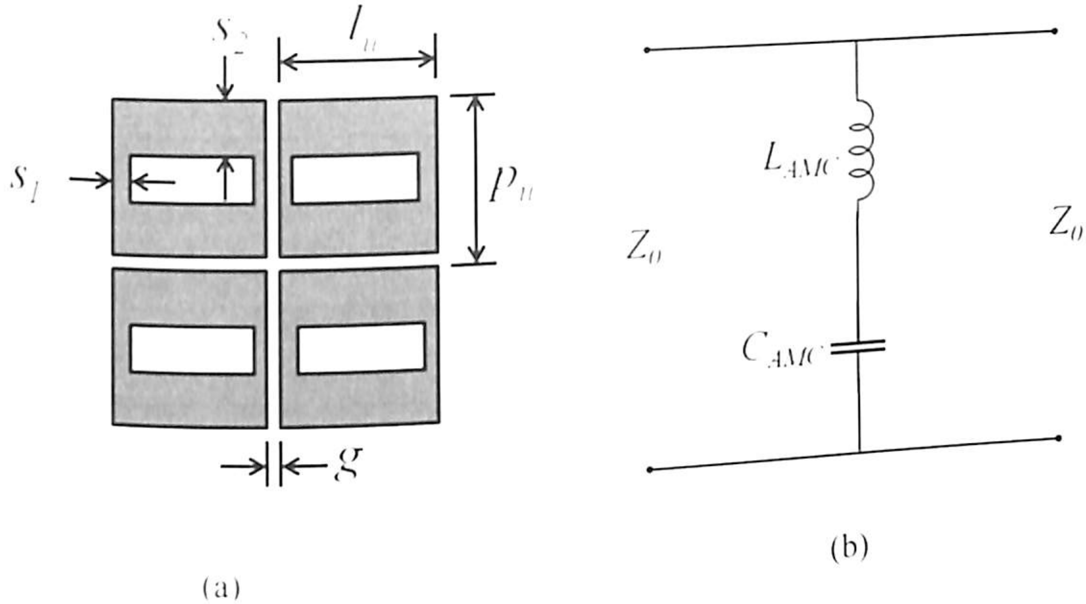

Figure 4.12. Loop AMC (a) Design with dimension (b) CM.

The design parameter of square loop AMC is shown in Figure 4.12(a). The FR-4 substrate with thickness 1.5 mm is used to support the designed AMC array.

The circuit model (CM) is developed to analyse the loop AMC unit cell with a simple and quick technique. The equivalent circuit with lumped components i.e. inductance (L_{AMC}) and capacitance (C_{AMC}) of a loop AMC unit cell is shown in Figure 4.12(b).

In case of incident transverse magnetic (TM) wave, the vertical grating of loop acts as a C_{AMC}, while the horizontal strips as a L_{AMC}. The values of C_{AMC} and L_{AMC}, are calculated using (4.3) and (4.3) as given in (Ferreira 2015), where l_u, p_u, s_1, s_2, and g are the loop AMC unit cell dimensions as shown in Figure 4.12. Since, s_1 and s_2 are is along horizontal strips and vertical strips respectively, so s_1 is used for TE mode and s_2 is used for TM mode wave incidence for calculation of L_{AMC}. θ_i is the incidence angle with respect to the normal to the plane of AMC. The following expressions are rewritten for TM mode as given in (Ferreira 2015).

$$\frac{X_{L_{AMC}}}{Z_0} = \omega L_{AMC} = \frac{l_u}{p_u} cos(\theta_i) F(p_u, 2s_2, \lambda, \theta_i) \quad (4.3)$$

$$\frac{B_{C_{AMC}}}{Y_0} = \omega C_{AMC} = 4\frac{l_u}{p_u} sec(\theta_i) F(p_u, g, \lambda, \theta_i)\varepsilon_e \quad (4.4)$$

where,

$$F(p_u, w, \lambda, \theta_i) = \frac{p}{\lambda}\left[ln\left(cosec\left(\frac{\pi w}{2p_u}\right)\right) + G(p_u, w, \lambda, \theta_i)\right] \quad (4.5)$$

$$G(p_u, w, \lambda, \theta_i) = \frac{1}{2} \times \frac{(1-\beta^2)^2\left[\left(1-\frac{\beta^2}{4}\right)(A_1+A_2)+4\beta^2 A_1 A_2\right]}{\left(1-\frac{\beta^2}{4}\right)+\beta^2\left(1-\frac{\beta^2}{2}-\frac{\beta^4}{8}\right)(A_1+A_2)+2\beta^6 A_1 A_2} \quad (4.6)$$

$$A_{1,2} = \frac{1}{\sqrt{\left[1 \pm \frac{2p_u \sin\theta_i}{\lambda} - \left(\frac{2p_u \cos\theta_i}{\lambda}\right)^2\right]}} - 1 \quad (4.7)$$

$$\beta = \sin\left(\frac{\pi w}{2p_u}\right) \quad (4.8)$$

The factor ε_e for square loop AMC was introduced in (Munk 2000). An AMC with dimensions l_u = 18 mm, s_1 = 1.5 mm, s_2 = 5 mm, and g = 0.15 mm are assumed to provide transmission for WLAN range.

To analyse the AMC unit cell on S_{21} (dB) transmission characteristics, the value of parameters l_u, s_2, and g are varied, while keeping p_u = 18.5 mm. Significant changes are visible when l_u varies from 17.8 mm to 18.4 mm with the step of 0.2 mm, as depicted in Figure 4.13. Since p_u is constant, so $g = p_u - l_u$ also changes with l_u. When the value of s_2 is increased from 1 mm to 5 mm, the stop band shifts from 2.1 GHz to 5.2 GHz with increase in the bandwidth of the stop band as may be seen in Figure 4.14. The values of lumped elements of square loop AMC calculated for TM wave incidence using equation (4.3) and (4.4) for variation given in Figure 4.13 and Figure 4.14 are indicated in Table 4.2 and Table 4.3.

Table 4.2. Calculated values of lumped elements of loop AMC with pu = 18.5 mm, s_2 = 5 mm, h = 1.5 mm and p_u = 18.5 mm, at ε_r = 4.4, ε_{eff} = 2.7 and θ_i = 0°.

lu (mm)	g (mm)	L_{AMC} (nH)	C_{AMC} (pF)	Frequency (GHz)
17.8	0.7	1.06	0.78	5.5
18	0.5	1.07	0.88	5.2
18.2	0.3	1.08	1.03	4.8
18.4	0.1	1.08	1.34	4.2

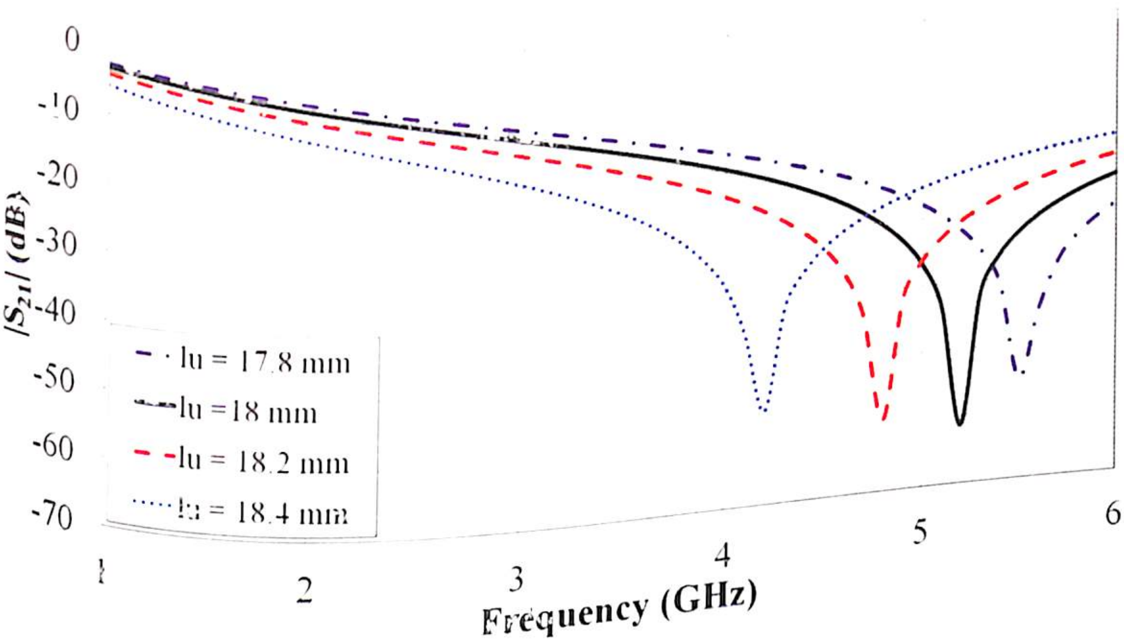

Figure 4.13. Influence of l_u parameter on loop AMC unit cell frequency response, with s_2 = 5 mm, and p_u = 18.5 mm at θ_i = 0°.

The observations based on CST simulations such as the influence of parameters g, p_u, and l_u on S_{21} (dB) characteristics assisted in the development of circuit model as demonstrated earlier in Figure 4.12(b). The circuit model S_{21} characteristics is compared with the CST S_{21} characteristics and shown in Figure 4.15. The CST S_{21} (dB) characteristics results demonstrate the validity of the circuit model, which estimates the frequency response of AMC structure.

Table 4.3. Calculated values of lumped elements of loop AMC with $g = 0.5$ mm, $l_u = 18$ mm, $h = 1.5$ mm and $p_u = 18.5$ mm, at $\varepsilon_r = 4.4$, $\varepsilon_{eff} = 2.7$ and $\theta_i = 0°$.

s_2 (mm)	L_{AMC} (nH)	C_{AMC} (pF)	Frequency (GHz)
1	6.43	0.87	2.1
2	4	0.87	2.7
3	2.63	0.87	3.3
4	1.72	0.87	4.1
5	1.07	0.88	5.2

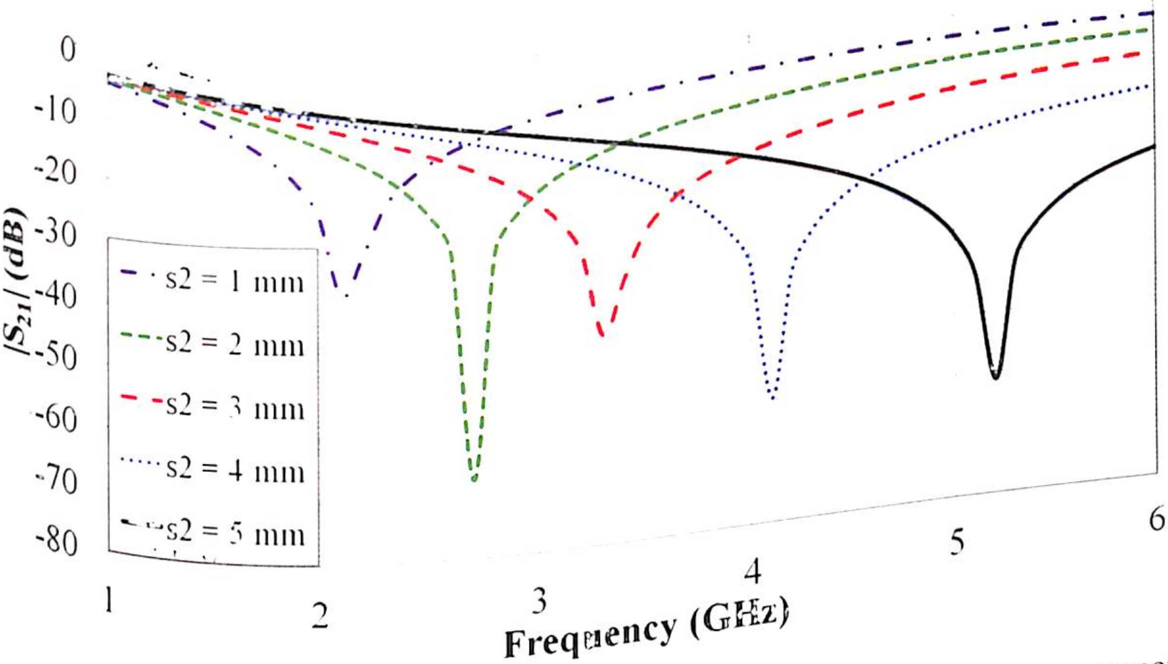

Figure 4.14. Influence of s_2 parameter on loop AMC unit cell frequency response, with $l_u = 18$ mm and $g = 0.5$ mm at $\theta_i = 0°$.

The square loop unit cell element, with edge length $l_u = 18$ mm, within a AMC has different inner edge widths, $s_1 = 1.5$ mm and $s_2 = 5$ mm with an inter-element spacing of 0.5 mm has been selected to form a 2×2 AMC element array as shown in Figure 4.12(a). The correction factor ε_{corr} available in (Ferreira 2015), provide large error for frequency calculation for TM incidence wave. The $\varepsilon_e = 0.5\ (\varepsilon_r+1)$ (Munk 2000) provide less error in band stop frequency calculation of loop AMC which will be well suited for TM wave incidence.

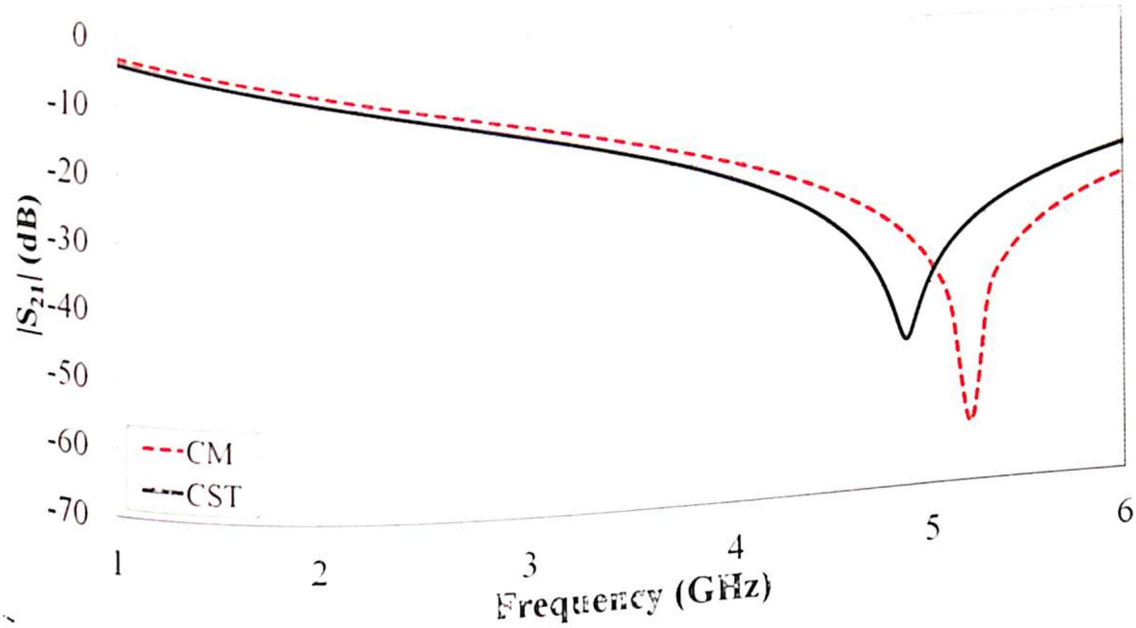

Figure 4.15. Comparison of loop AMC unit cell S21 (dB) CM result with CST results.

In case of incident transverse electric (TE) wave, the vertical strips of loop act as a L_{AMC}, while the horizontal gratings as a C_{AMC}. Equations (4.3) and (4.4) can be rewritten with functions $F(p_u, 2s_1, \lambda, \theta_i)$, $F(p_u, g, \lambda, \theta_i)$ to calculate the ωL_{AMC} and ωC_{AMC} respectively. The series lumped elements L_{AMC} and C_{AMC} given in Figure 4.12(b) will be changed to parallel connection in case of TE wave incidence as suggested in (Dubrovka 2006). The correction factor ε_{corr} available in (Ferreira 2015) for TE incidence, when applied to equation (4.4) provides better matching of CM and CST S_{21} results as may be observed in Figure 4.18.

To analyze the AMC unit cell on S_{21} (dB) transmission characteristics for TE mode, the value of parameters l_u, s_1, and g are varied, while keeping p_u = 18.5 mm. Significant changes are visible when l_u varies from 17.8 mm to 18.4 mm with the step of 0.2 mm, as depicted in Figure 4.16.

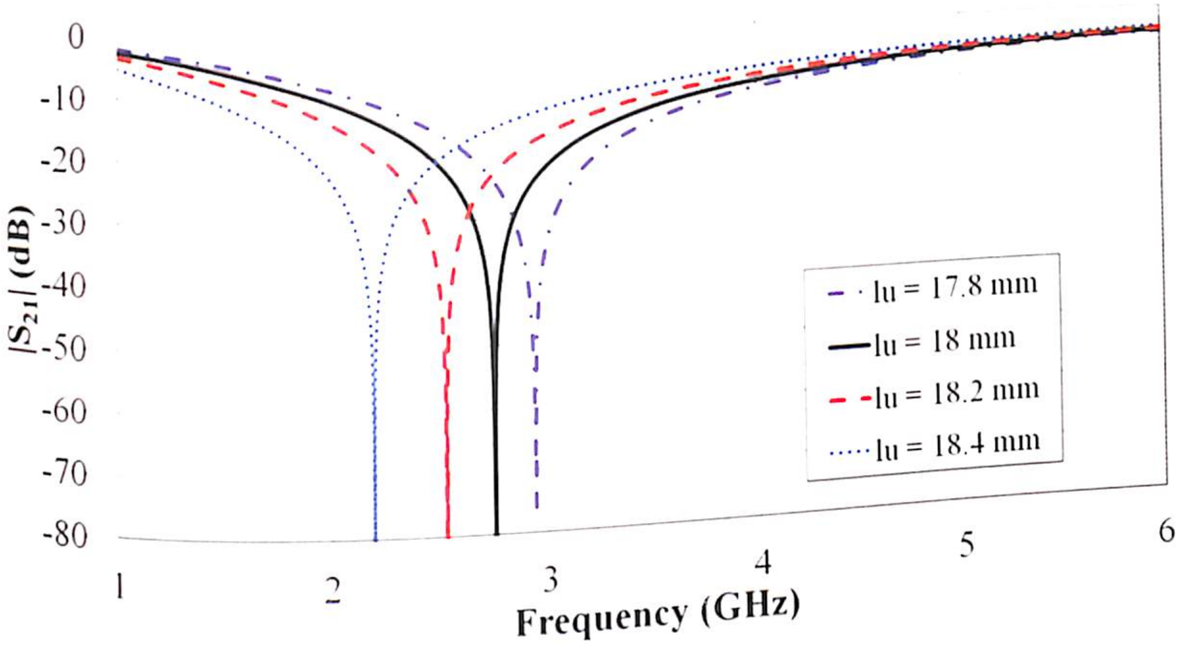

Figure 4.16. Influence of l_u parameter on loop AMC unit cell frequency response, with s_l = 1.5 mm, and p_u = 18.5 mm at $\theta_i = 0^\circ$.

Since p_u is constant, so $g = p_u - l_u$ also changes with l_u. When the value of s_l is increased from 1.5 mm to 6 mm with step of 1.5 mm, the stop band shifts from 2.4 GHz to 6.5 GHz with increase in the bandwidth of the stop band as may be seen in Figure 4.17. The values of the L_{AMC} and C_{AMC} are calculated for TE wave incidence and presented in Table 4.4 and Table 4.5.

Table 4.4. Calculated values of lumped elements of loop AMC with p_u = 18.5 mm, s_l = 1.5 mm, h = 1.5 mm, at ε_r = 4.4, ε_{corr} = 2.08 and $\theta_i = 0^\circ$.

l_u (mm)	g (mm)	L_{AMC} (nH)	C_{AMC} (pF)	Frequency (GHz)
17.8	0.7	4.96	0.59	2.9
18	0.5	5.01	0.67	2.7
18.2	0.3	5.06	0.79	2.5
18.4	0.1	5.1	1.03	2.2

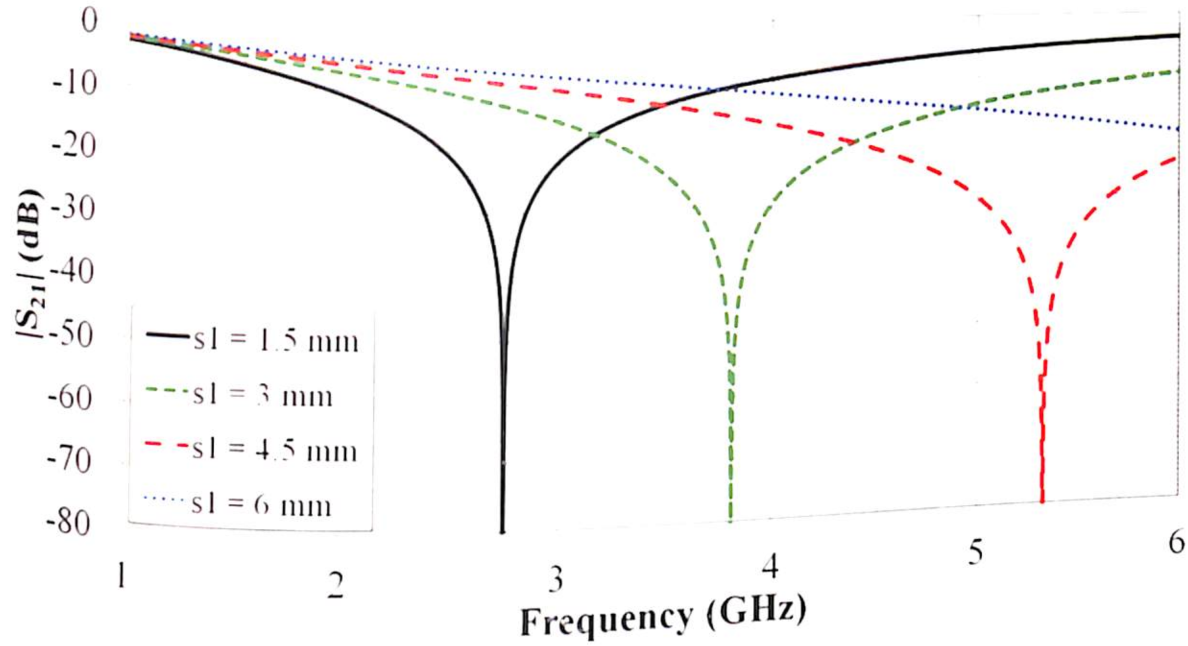

Figure 4.17. Influence of s_1 parameter on loop AMC unit cell frequency response, with l_u = 18 mm and g = 0.5 mm at $\theta_i = 0^\circ$.

Table 4.5. Calculated values of lumped elements of loop AMC with g = 0.5 mm, lu = 18 mm, h = 1.5 mm and p_u = 18.5 mm, at ε_r = 4.4, and $\theta_i = 0^\circ$.

s_l (mm)	ε_{corr}	L_{AMC} (nH)	C_{AMC} (pF)	Frequency (GHz)
1.5	2.08	5.01	0.67	2.7
3	2.04	2.64	0.66	3.8
4.5	1.98	1.38	0.65	5.3
6	1.89	0.61	0.64	8

The circuit model S_{21} characteristics are compared with the CST and measured S_{21} characteristics and shown in Figure 4.18. The CST S_{21} (dB) characteristics results demonstrate the validity of the circuit model, which estimates the frequency response of AMC structure.

The square loop unit cell element, with edge length l_u = 18 mm, within a AMC has different inner edge widths, s_1 = 1.5 mm and s_2 = 5 mm with an inter-element spacing of 0.5 mm has been selected to form a 2×2 AMC element array as shown in Figure 4.12(a).

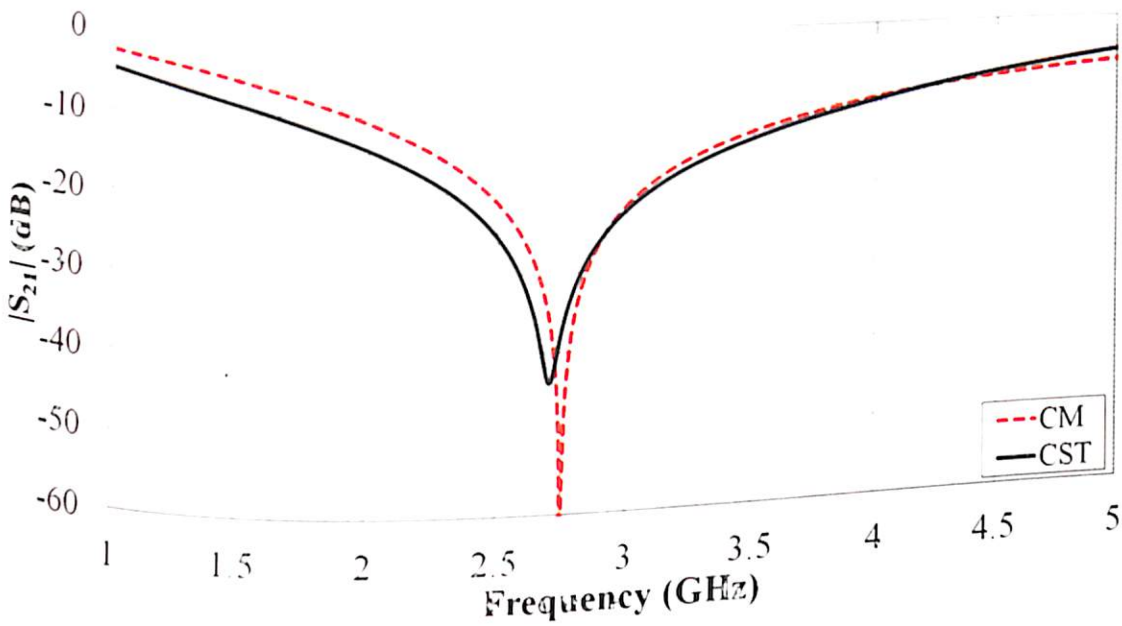

Figure 4.18. Comparison of loop AMC unit cell S_{21} (dB) CM result with CST results.

4.4. Probe-Fed Wideband AMC-integrated Hexagonal S-Band Antenna

Multilayered dielectric is used to assemble the AMC integrated hexagonal antenna as shown in Figure 4.19. Layer 1 (lower layer) and 2 (upper layer) with dimensions 60 × 60 mm^2 have a dielectric constant of 3.7 with heights, h_{amc} and h with values 3 mm and 4.5 mm respectively. Both layers are formed by stacking and bonding two and three layers of commercially available FR-4 substrate with thickness 1.5 mm. For bonding the multilayer stack, cynoacrylate instant adhesive ($2 \le \varepsilon_r \le 3.5$, $0.033 \le \tan\delta \le 0.036$) is used. Due to application of adhesive, the effective ε_r drops to 3.7 for substrate from 4.3. The layer 1 backed with ground plane 50 × 50 mm^2 supports the AMC array. The hexagonal patch antenna with PPC is supported by layer 2. The assembled stacked arrangement of the integrated antenna is shown in Figure 4.19(a) and can be visualized through cross-section along the X-axis as shown in Figure 4.19(b).

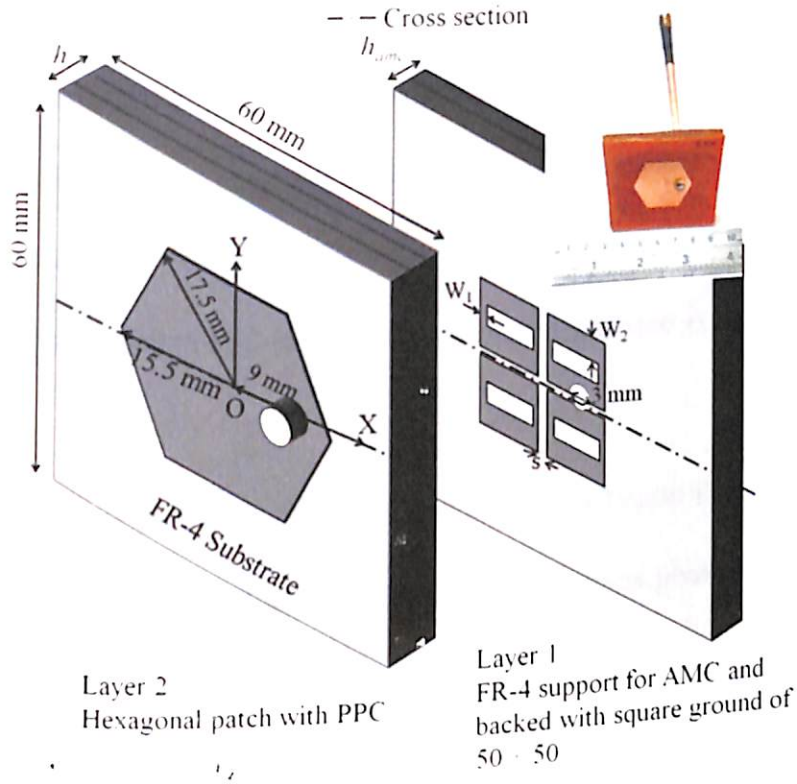

(a)

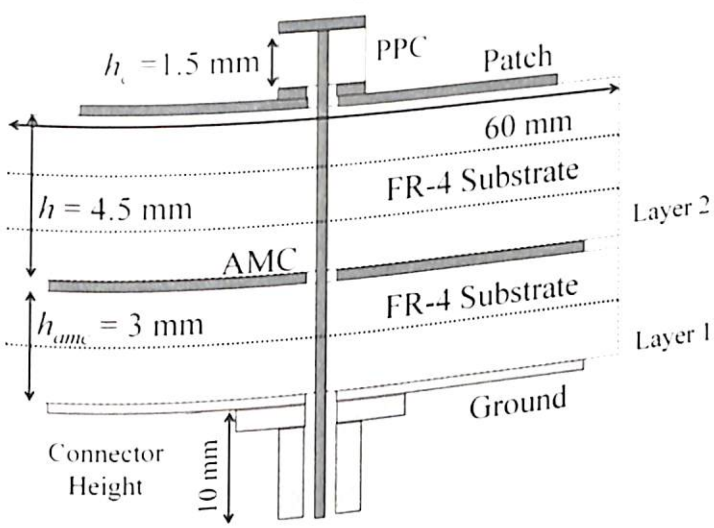

(b)

Figure 4.19. (a) Assembly of probe compensated AMC integrated hexagonal antenna [Antenna photograph in Inset] (b) Cross sectional view.

The circular PPC used to match impedance with probe reactance developed due to thick substrate is an additional feature of the AMC integrated antenna which results in radiation mode purity. Double sided copper clad with FR-4 dielectric as substrate of radius 2.4 mm and height, h_c = 1.5 mm along with a concentric circular via for SMA pin forms a PPC.

Variety of AMC designs for various antenna applications are studied and analyzed in (Dewan 2017). To widen the bandwidth of hexagonal antenna the loop AMC design without vias is selected after preliminary analysis. The square loop unit cell element, with edge length = 17.8 mm, within a 2×2 AMC array has different inner edge widths, W_1 = 3 mm and W_2 = 10 mm with an inter-element spacing of 0.7 mm as shown in Figure 4.19(a). The photograph of the fabricated and assembled AMC integrated hexagonal antenna is shown in Figure 4.19(a) [Inset].

The 2×2 AMC element array sandwiched between FR-4 layers is simulated at 0° incident angle of the transverse magnetic (TM) wave and the reflection phase is observed between 2 to 3 GHz. The layer 1 and layer 2 heights i.e. h_{amc} and h respectively are optimized for zero phase shift condition so that there will be constructive interference between the incident and the reflected wave, since phase difference is zero degree ($\phi_{incident}$ - $\phi_{reflected}$ = 0°), as expressed in (Yang 2013). The reflection phase bandwidth of AMC array observed between +90° to -90° which ranges from 2.25 to 2.51 GHz as may be explicitly seen in Figure 4.20.

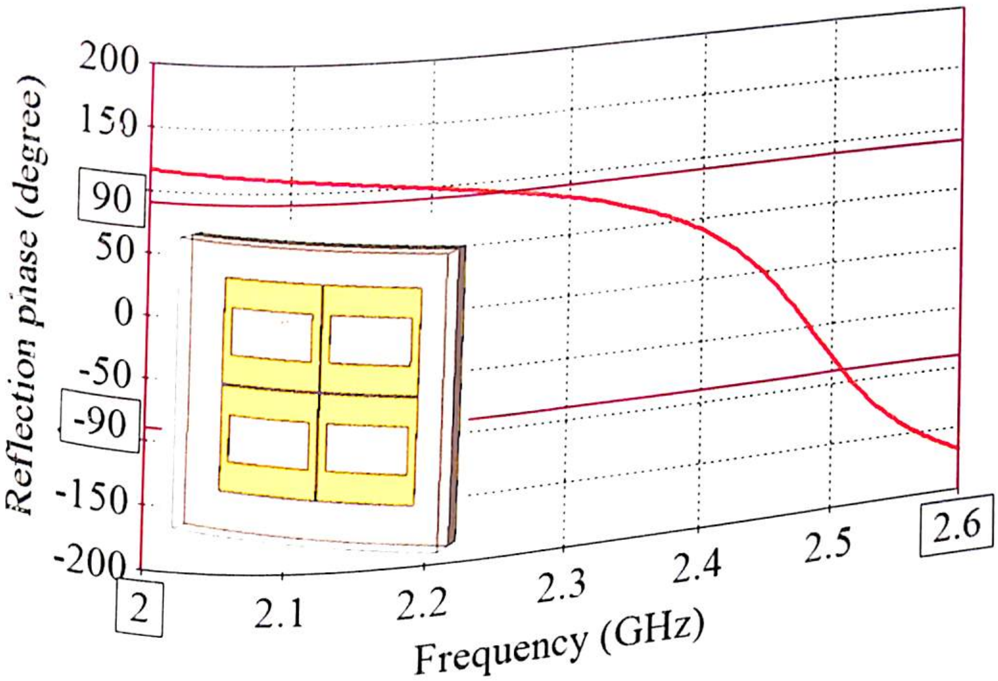

Figure 4.20. Reflection phase versus frequency of the AMC.

The simulated result suggest that the AMC act as reflector at 2.4 GHz and AMC array reflection phase bandwidth is sufficient enough to integrate within the hexagonal antenna to widen the radiation bandwidth.

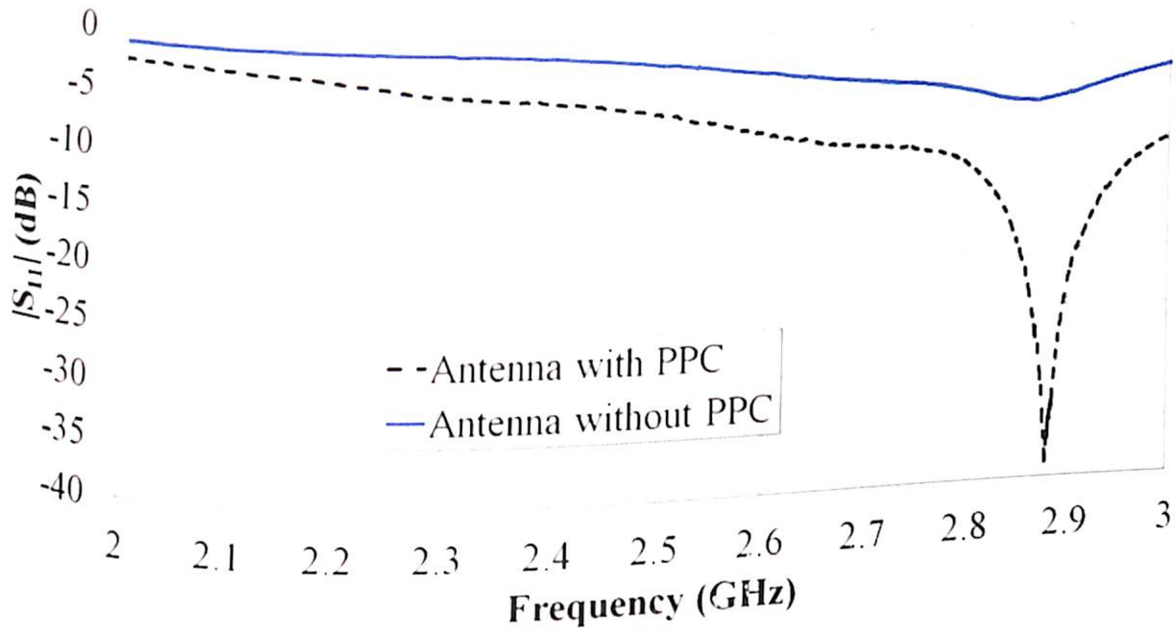

(a)

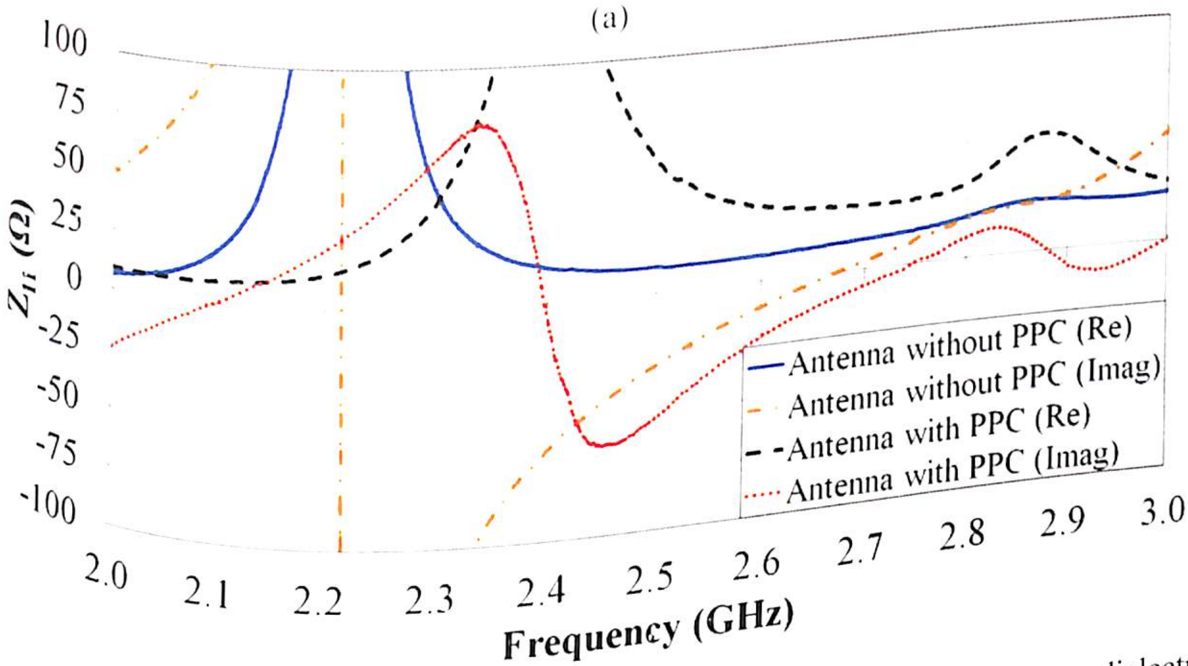

(b)

Figure 4.21. Measured results of the antenna 1 with AMC array and air as dielectric (h_{air} = 3 mm) (a) S_{11} (dB) (b) Z_{11} (Ω).

A vector network analyser (VNA) (Keysight N9928A) is used to measure the return loss of the fabricated antenna. To understand the effect of PPC, AMC array and the substrate thickness, three antenna prototypes are fabricated. In all the three antenna prototypes the hexagonal patch antenna, the PPC and the ground dimension are same as shown in Figure 4.21. The first antenna prototype (antenna 1) consists of an AMC array and a combination of dielectrics (FR-4 + air) below hexagonal patch and above AMC array. The heights of the dielectric layers are 1.5 mm for FR-4 and 3 mm for air respectively. The return loss of antenna 1 is measured with and without PPC and it is observed that PPC with radius 2.4 mm is matching the impedance at resonating frequency at 2.88 GHz with impedance bandwidth of 340 MHz. The combination of air and FR-4 dielectric is shifting the desired resonating frequency from 2.45 GHz to 2.88 GHz as shown in Figure 4.21(a). The real part of impedance changes from 21.8 Ω to 51 Ω at the operating frequency of antenna 1, 2.88 GHz while the imaginary part changes from 20.37 Ω to 0.07 Ω as observed from Figure 4.21(b) when PPC is connected.

In second antenna prototype (antenna 2), the AMC array is removed and the air dielectric is replaced by FR-4 of 3 mm to form an overall dielectric with an effective height, h = 7.5 mm ($0.06\lambda_0$~$0.1\lambda_0$) between the hexagonal patch and the ground plane. Return loss for antenna 2 is measured and similar observation of PPC matching the impedance is observed but due to replacement of air dielectric with FR-4 of effective height 7.5 mm, the bandwidth of the antenna is enhanced to 623 MHz at 2.88 GHz due to absence of AMC as may be observed in Figure 4.22(a). The frequency axis in Figure 4.20 is extended to 3.5 GHz to accommodate the wide operating band of antenna 2. Probe compensation effect is visible in case of antenna 2 where impedance changes from 97 - j 6.81 Ω to 46.13 - j 4.94 Ω at 2.88 GHz when PPC is present as may be observed from Figure 4.22(b).

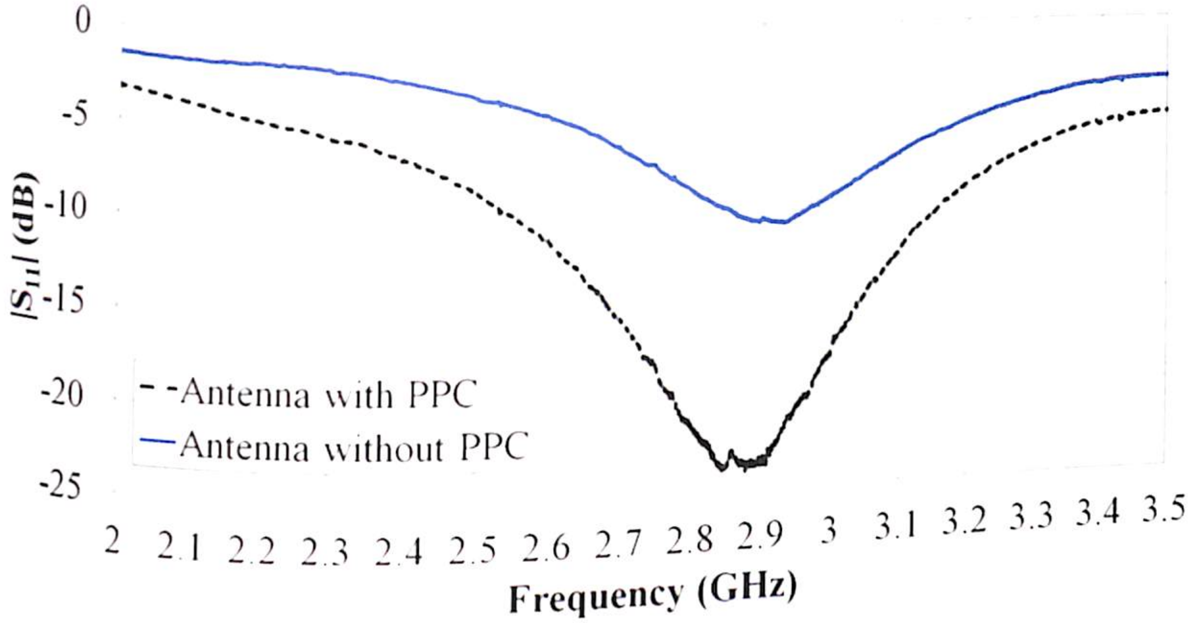

(a)

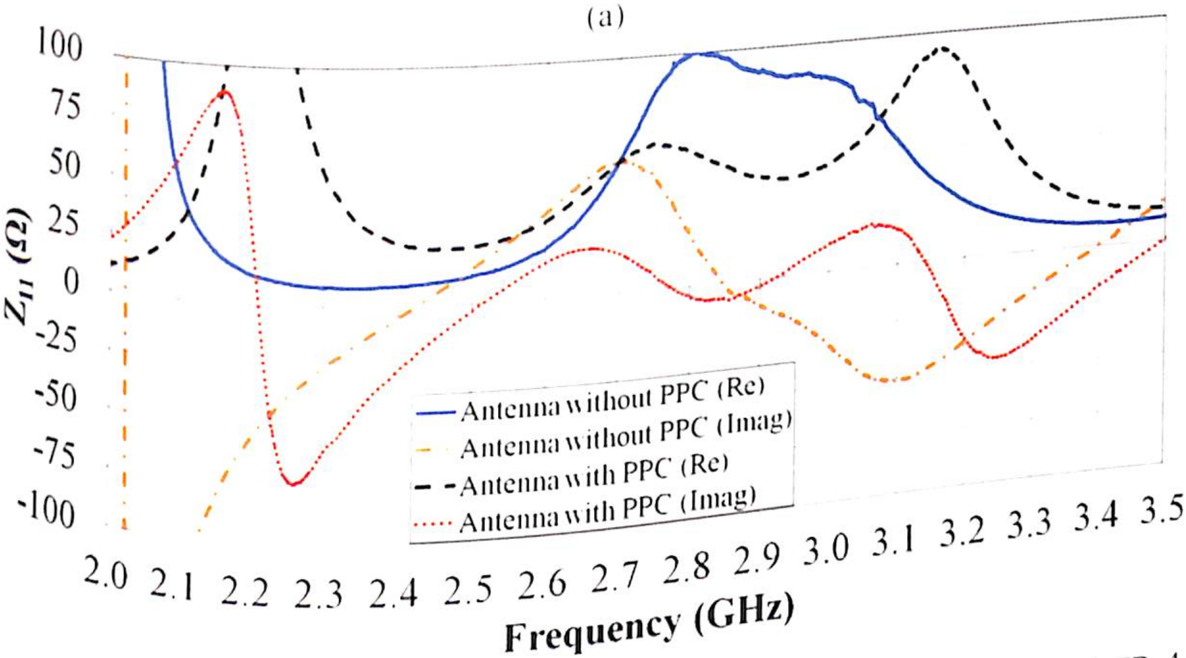

(b)

Figure 4.22. Measured results of the antenna 2 without AMC array and FR-4 as dielectric (h = 7.5 mm) (a) S_{11} (dB) (b) Z_{11} (Ω).

The final prototype (antenna 3) is same as shown in Figure 4.23(a) i.e. antenna with AMC and FR-4. The measured bandwidth of the antenna 3 ranges from 2.24 to 2.58 GHz. The measured return loss of fabricated antenna with PPC and fabricated antenna without PPC is compared in Figure 4.23(a). It can be observed from Figure 4.23(b) that PPC is again matching the impedance of fabricated antenna with inductive probe developed due to thick substrate. In case of antenna 3, the real part of the impedance varies from 27.3 Ω to 64.91Ω while imaginary part changes from -7.5 Ω to -13.3 Ω in presence of PPC.

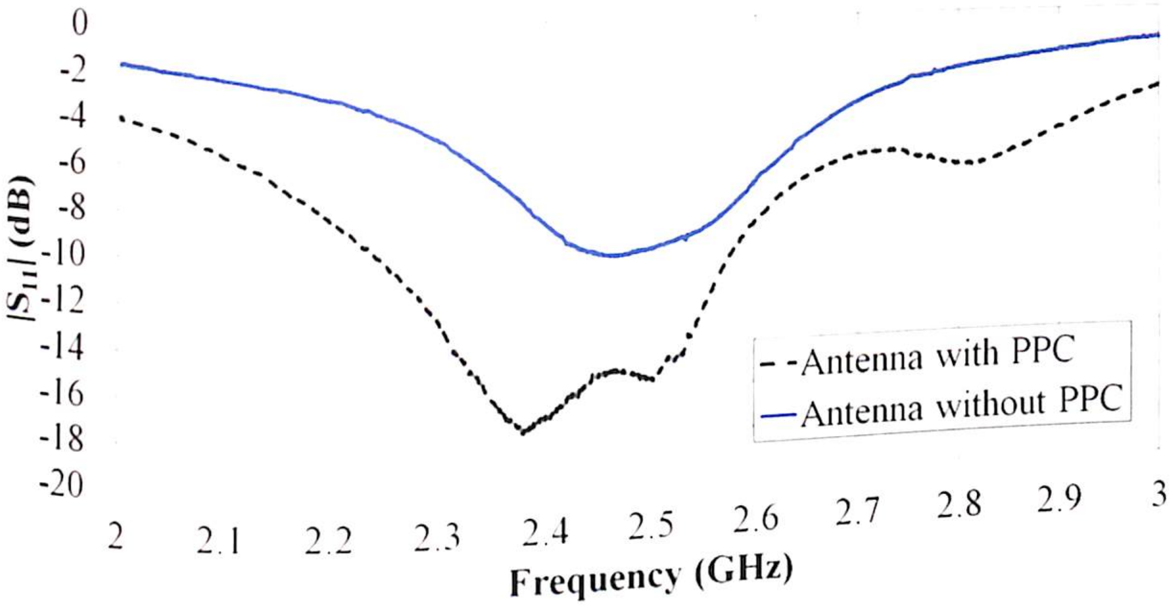

(a)

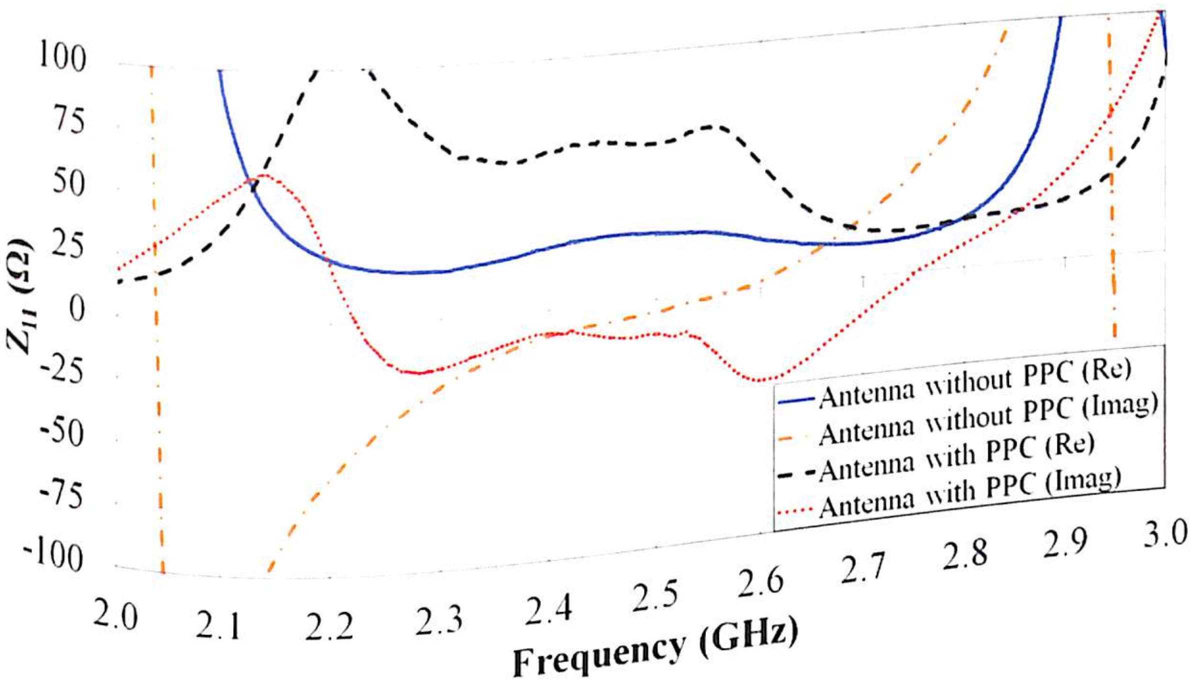

(b)

Figure 4.23. Measured results of the antenna 3 with AMC array and FR-4 as dielectric (h = 4.5 mm) (a) S_{11} (dB) (b) Z_{11} (Ω).

Figure 4.21(b), Figure 4.22(b) and Figure 4.23(b) suggests that the PPC with same dimensions for three different prototypes i.e. antenna 1, antenna 2 and antenna 3 does not provide similar inductive probe compensation. Desired inductive compensation can be achieved by adjusting the dimension of PPC to match 50 Ω impedance. Although perfect matching of impedance is sensitive to PPC placement and fabrication tolerances, it is still a suitable technique to overcome impedance mismatch in probe-fed antennas.

The impedance of the AMC array is high due to small tangential magnetic field along the surface of AMC array within the operating bandwidth of fabricated antenna with PPC. It is also interesting to note that the AMC is limiting the bandwidth of the antenna due to small reflection phase bandwidth as observed from Figure 4.21(a) and 4.23(a). Bandwidth of 340 MHz is observed in Figure 4.21(a) and 4.23(a) i.e. with and without air as dielectric respectively but without AMC it should have been high as suggested through results presented in Figure 4.22(a). Although AMC is restricting the bandwidth of the antenna 3, but it is also tuning antenna to the desired resonant frequency of 2.45 GHz. AMC is actually compensating high substrate thickness required at low resonant frequency.

Pre-calibrated standard UWB horn is used to measure the absolute gain of the fabricated antenna with PPC. The farfield gain of the fabricated antenna is unidirectional for both orthogonal principal planes, $\phi = 0°$ (E-plane) and $\phi = 90°$ (H-plane) as may be observed from Figure 4.24. The farfield gain of the fabricated antenna is stable within the radiation bandwidth as observed during measurement. The fabricated antenna has a measured peak gain of 3.14 dB at 2.4 GHz for E and H-plane respectively. The 3-dB beamwidth of the antenna are 90° and 80° for E and H-plane respectively for the main lobe direction at 0°. The cross polarization level is below -13 dB and -11 dB for E and H-plane as reflected in Figure 4.24. Although it appears that the cross polarization is high in H-plane but the minimum value at gain axis in Figure 4.24(a) differs to that of Figure 4.24(b). The farfield gain of the fabricated antenna is sufficient enough within the operating bandwidth for Wi-Fi application. Back lobe is present in the radiation pattern of antenna without AMC presented in Figure 4.11. Due to introduction of AMC the back lobe diminishes as observed from Figure 4.24.

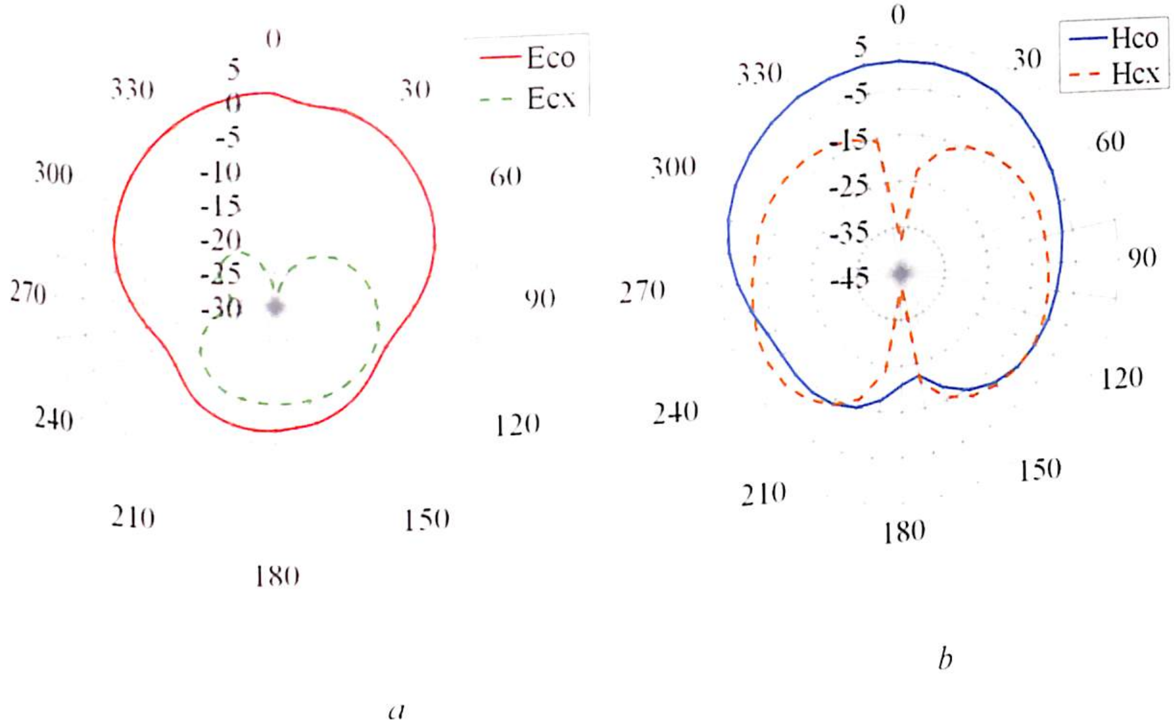

Figure 4.24. Measured Farfield Gain (dB) (Co and Cross Polar) of the antenna integrated with AMC at 2.4 GHz (a) E-plane (b) H-plane.

4.5. Conclusion

A technique to compensate probe reactance to excite lower mode in a hexagonal patch antenna is demonstrated. A PPC is used with feeding probe to excite the lower mode by matching the impedance at 2.4 GHz. The antenna, exhibits a gain of 2.11 dB at 2.4 GHz in main lobe direction. The farfield measurement results show that the designed antenna has good separation between co-and cross-polar fields at 0° boresight. The slotted hexagonal antenna with PPC is compact in structure and may be used for various S-band applications.

A low profile probe compensated AMC-integrated hexagonal antenna for S-Band applications like Wi-Fi has been presented. The fabricated antenna demonstrates a wide radiation bandwidth of 340 MHz covering Wi-Fi applications by preserving radiation purity which results due to presence of PPC and AMC integration. The antenna farfield gain is greater than 0 dB over a band of 2.24 to 2.58 GHz, with a peak gain of 3.14 dB at 2.4 GHz which make it definitely suitable for Wi-Fi applications.

The techniques presented in this chapter of the thesis leads to uniform radiation pattern due to fundamental mode excitation and wide bandwidth due to thick substrate and AMC. There are the desired attribute when the low profile patch antenna is designed. The AMC reflector technique is further exploited in the subsequent chapter for the boresight gain enhancement of probe fed hexagonal monopole antenna. Also the technique demonstrated in this chapter of the thesis will be utilized in the next chapter when probe fed hexagonal patch antenna is integrated with AMC reflector.